



17 **Abstract**

18 Fire frequency and severity are increasing in high latitude regions, but the degree to which  
19 groundwater flow impacts the response of permafrost to fire remains poorly understood and  
20 understudied. Here, we use the Anaktuvuk River Fire (Alaska, USA) as an example to simulate  
21 groundwater-permafrost interactions following fire. We identify key thermal and hydrologic  
22 parameters controlling permafrost and active layer response to fire both with and without  
23 groundwater flow, and separate the relative influence of changes to the water and energy  
24 balances. Our results show that mineral soil porosity, which influences the bulk subsurface  
25 thermal conductivity, is a key parameter controlling active layer response to fire in both the  
26 absence and presence of groundwater flow. However, neglecting groundwater flow increases the  
27 perceived importance of subsurface thermal properties, such as the thermal conductivity of soil  
28 solids, and decreases the perceived importance of hydrologic properties, such as the soil  
29 permeability. Furthermore, we demonstrate that changes to the energy balance (increased soil  
30 temperature) are the key driver of increased active layer thickness following fire, while changes  
31 to the water balance (decreased groundwater recharge) lead to reduced landscape-scale  
32 variability in active layer thickness and groundwater discharge to surface water features. These  
33 results indicate that explicit consideration of groundwater flow is critical to understanding how  
34 permafrost environments respond to fire.

35 **Plain Language Summary**

36 While scientists know that fire often causes permafrost (areas of permanently frozen ground) to  
37 thaw, the degree to which the movement of groundwater either enhances or reduces this thawing  
38 process is not well understood. In this study, we simulate the response to permafrost to fire using  
39 models that both include and ignore groundwater flow while varying different model input  
40 datasets. Our results show that, when groundwater flow is ignored, the relative importance of soil  
41 properties associated with heat movement may be overestimated, and the importance of soil  
42 properties associated with water movement are likely to be underestimated. Additionally, we  
43 show that increased soil temperature following fire is the most important factor deepening  
44 permafrost thaw each year (also known as the ‘active layer’). However, reductions in the amount  
45 of water recharging groundwater systems decreased differences in permafrost thaw depth  
46 between upland and lowland regions of a watershed, as well as the amount of groundwater that  
47 flows into surface water features such as streams.

48 **Index Terms:**

49 1829 Groundwater hydrology; 0475 Permafrost, cryosphere, and high-latitude processes; 0764  
50 Energy balance; 1655 Water cycles; 1846 Model calibration

51 **Keywords:**

52 tundra fire; Long-Term Ecological Research (LTER) network; active layer thickness; baseflow;  
53 Arctic; groundwater modeling;

## 54 **1 Introduction**

55 Fire frequency and severity in the Arctic are expected to increase in the future and can  
56 have large-scale and long-lasting effects (Flannigan et al., 2005; Hu et al., 2015). For instance,  
57 fire can change the landscape locally by enhancing erosion and thermokarst development  
58 (Chipman & Hu, 2017; Iwahana et al., 2016; Jones et al., 2015), and have global impacts by  
59 releasing soil carbon which contributes to global climate change (Abbott et al., 2016; Balshi et  
60 al., 2007). In permafrost settings, these changes are primarily driven by increases in the thickness  
61 of the active layer (the soil above the permafrost which thaws and refreezes annually) following  
62 fire. Therefore, understanding the processes underlying post-fire active layer dynamics is  
63 essential to anticipate and mitigate changes in the Arctic landscape as well as understand impacts  
64 on global carbon cycling.

65 Post-fire increases in active layer thickness occur via two mechanisms: (1) thinning the  
66 near-surface organic soil layer and reducing the thermal buffer between air and the subsurface;  
67 and (2) decreasing albedo which further increases in energy input into the subsurface (Brown et  
68 al., 2015, 2016; Iwahana et al., 2016; Kasischke & Johnstone, 2005; Rocha & Shaver, 2011b;  
69 Smith et al., 2015). Past modeling efforts studying post-fire active layer thickness have primarily  
70 concluded that soil thermal properties are the most important control of permafrost response to  
71 fire (Jiang et al., 2012, 2015b; Yi et al., 2009). However, these studies neglected the potential  
72 impacts of lateral groundwater flow on permafrost by using one-dimensional models (Brown et  
73 al., 2015; Jiang et al., 2015b; Treat et al., 2013; Yi et al., 2009; Zhang et al., 2003, 2015; Zhuang  
74 et al., 2002).

75 In contrast, however, field research suggests that hydrologic properties such as drainage  
76 patterns and soil properties such as texture influence permafrost response to fire (Kasischke et  
77 al., 2007; Minsley et al., 2016), implying that hydrological fluxes may be an important control on  
78 post-fire permafrost thaw. Increased subsurface hydrological connectivity, which is associated  
79 with thickening active layers, has been shown to lead to positive feedbacks on permafrost thaw  
80 by increasing advective heat transport via groundwater flow (Bense et al., 2009, 2012; Connon et  
81 al., 2014; Kurylyk et al., 2016; McKenzie & Voss, 2013; Walvoord et al., 2012), although this  
82 has not been studied in the context of fire. Similar processes could result in a positive post-fire  
83 feedback on permafrost degradation. However, the role of groundwater flow in mediating post-  
84 fire changes in active layer thickness is not well understood due to a lack of available data in  
85 high-latitude regions. Furthermore, no previous modelling work has investigated the importance  
86 of fire-induced feedbacks between groundwater flow and permafrost degradation.

87 To address this knowledge gap, this study explores the question, *how does groundwater*  
88 *flow impact permafrost response to fire?* To answer this question we use an archetypal modeling  
89 approach, where a real-world domain is simplified to isolate specific processes related to a  
90 research question of interest, rather than constructing a site-specific model (Zipper et al., 2018).  
91 Our models are driven by field observations from three sites along a burn severity gradient (i.e.  
92 severe, moderate, and unburned) following the 2007 Anaktuvuk River Fire (ARF), which was  
93 the largest recorded tundra fire in history (Mack et al., 2011). The sites exhibited a large gradient

94 in soil thermal dynamics that allowed us to address two specific sub-questions: (i) what is the  
95 relative importance of subsurface thermal and hydrologic properties governing post-fire active  
96 layer thickness, and how does their importance change in the presence or absence of  
97 groundwater flow?; and (ii) how do post-fire changes to the water balance and energy balance  
98 interact to influence active layer thickness and groundwater discharge to surface water features?

99 While previous work (cited above) has suggested that thermal properties are the key  
100 control on active layer thickness, we hypothesize that the importance of thermal properties is  
101 overestimated in previous modeling studies due to a lack of advective heat transport through  
102 groundwater flow. Therefore, when groundwater flow is considered, the relative importance of  
103 hydrologic properties as a control over active layer thickness will increase. Furthermore, we  
104 hypothesize that changes to the energy and water balance following fire will be opposite in  
105 directional effect, with increases in soil temperature increasing active layer thickness due to  
106 enhanced conduction of heat into the subsurface, but counteracted by decreases in groundwater  
107 recharge which reduce advective heat transport. Understanding the response of permafrost and  
108 subsurface hydrology to fire is key to predicting and planning for future change in the water and  
109 energy balances of cold regions, particularly since fire effects will be superimposed on a  
110 warming trend which is already contributing to permafrost thaw across the Arctic (Hu et al.,  
111 2015; Lique et al., 2016; Walvoord & Kurylyk, 2016; Wrona et al., 2016).

## 112 **2 Methodology**

### 113 *2.1 Anaktuvuk River Fire*

114 The ARF burned ~1000 km<sup>2</sup> of Alaska's North Slope from July through October of 2007,  
115 making it the largest recorded tundra fire in Alaska's history (Jones et al., 2009). The ARF is  
116 thought to be an analog for a future Arctic in which warmer temperatures and expanding shrub  
117 lead to more large fires such as the ARF, though future climate impacts on Arctic fire regimes  
118 are highly uncertain (Higuera et al., 2008; Hu et al., 2010, 2015). Additionally, the severity of  
119 the fire varied over the large area burned, providing a gradient of burn severity which can be  
120 used to relate the ARF to fires of varying magnitudes elsewhere. Finally, the ARF has been  
121 studied in detail due to its proximity to the Toolik Lake Long-Term Ecological Research (LTER)  
122 station, providing a rich interdisciplinary body of knowledge in which to situate our study (Bret-  
123 Harte et al., 2013; De Baets et al., 2016; Jiang et al., 2015a, 2017; Mack et al., 2011; Rocha &  
124 Shaver, 2011a).

125 In the present study, we use three sites across a burn severity gradient which were  
126 instrumented with eddy covariance towers in June 2008, which we will refer to as Unburned  
127 (UB; 68.99°N, 150.28°W), Moderate Burn (MB; 68.95°N, 150.21°W), and Severe Burn (SB;  
128 68.93°N, 150.27°W). The UB site is tundra tussock which was not affected by the fire; the MB  
129 site is a mix of partially and completely burned areas; and all vegetation was burned at the SB  
130 site (Rocha & Shaver, 2009, 2011a). Following the ARF, a decrease in soil organic layer  
131 thickness and albedo led to higher summer soil temperature at the MB and SB sites relative to

132 UB baseline; and evapotranspiration increased due to surface ponding following the loss of soil  
133 organic matter (Jiang et al., 2015b; Rocha & Shaver, 2011b).

## 134 *2.2 Modeling approach*

135 To test our hypotheses (Section 1), we used a suite of numerical model simulations that  
136 are representative of the ARF sites. We use the modified version of the SUTRA numerical model  
137 (Voss & Provost, 2010) described in McKenzie et al. (2007) and McKenzie & Voss (2013). The  
138 modified model simulates saturated groundwater flow including freeze/thaw processes, which  
139 impact subsurface hydrologic and thermal properties based on the relative composition of three  
140 materials: liquid water, solid water (ice), and matrix material (soil solids).

141 Our guiding principle in model design was that of parsimonious archetypal modeling, or  
142 making a groundwater flow model in “the simplest way possible that captures the most important  
143 overall behavior” (Voss, 2011b, p. 1456). Thus, rather than building a site-specific calibrated  
144 model, we made several simplifying assumptions to isolate the aspects of the domain most  
145 relevant to our research questions (Zipper et al., 2018). At a high level, we simplified the  
146 landscape to a two-dimensional cross-section with a fully saturated subsurface, which is common  
147 when modeling groundwater-permafrost interactions (Ge et al., 2011; Kurylyk et al., 2016;  
148 McKenzie et al., 2007; McKenzie & Voss, 2013; Wellman et al., 2013). Specific assumptions  
149 related to the domain, boundary conditions, and model inputs are described in the sections  
150 below, and we discuss the potential implications of these assumptions in Section 4.4.

151 In our model, permeability is defined for the solid matrix material, and reduced as a  
152 function of liquid pore-water saturation using a relative permeability scaling coefficient. This  
153 coefficient is multiplied by the solid matrix permeability to obtain the effective permeability. We  
154 simulated saturated groundwater flow only, meaning that liquid pore-water saturation decreases  
155 when ice forms due to pore-water freezing. In our models, relative permeability decreases  
156 linearly as a function of decreasing liquid pore-water saturation to a minimum relative  
157 permeability value of  $10^{-8}$  following Kurylyk et al. (2016), McKenzie et al. (2007), and  
158 McKenzie & Voss (2013). Alternative approaches to reducing hydraulic conductivity as a  
159 function of soil ice content are reviewed in Kurylyk & Watanabe (2013) and include theoretical  
160 approaches (e.g. Lebeau & Konrad, 2010; Watanabe & Flury, 2008) and approaches based on the  
161 soil water characteristic curve for a drying soil (e.g. Brooks & Corey, 1964; Clapp &  
162 Hornberger, 1978; Van Genuchten, 1980). The onset of pore water freezing at a node occurs  
163 when temperature drops below 0 °C, and the proportion of frozen pore water increases linearly  
164 until a threshold temperature is reached (set here as -2 °C; McKenzie & Voss, 2013). At and  
165 below this threshold temperature, liquid water content is equal to a minimum allowed residual  
166 liquid water content (set here as 1% of pore space). Parameter values used in our simulation are  
167 defined in Table 1. For a full description of the model the reader is referred to McKenzie et al.  
168 (2007) and McKenzie & Voss (2013).

169

170

171 **Table 1.** Thermal and hydrologic properties of the numerical model. Parameters where value varied  
 172 between 1D and 2D simulations are noted. Bold values are varied in sensitivity analysis (Section 2.2.3).

<b>Parameter</b>	<b>Value</b>	<b>Source/Notes</b>
<i>Discretization</i>		
Width (x dimension)	1D: 5 m 2D: 200 m	200 m is typical watershed half-width for Anaktuvuk River Fire region
Height (y dimension)	1D: 20 m 2D: 25 m to 20 m	Model height based on thermal bottom boundary condition (Section 2.2.2)
Slope	1D: 0% 2D: 2.5%	(Rocha & Shaver, 2011b)
Model Discretization (x)	5 m	
Model Discretization (y)	0.03 m (top) to 2.0 m (bottom)	
Number of Nodes/Elements	1D: 453/300 2D: 4961/4800	
Model Duration	6935 days	19 years (1998-2016), ignoring leap years
Model Timestep	1 day	
<i>Thermal Properties</i>		
<b>Organic soil solid thermal conductivity</b>	<b>0.25 to 0.69 W m<sup>-2</sup> °C<sup>-1</sup></b>	Literature values for peat (Jafarov et al., 2013; Kurylyk et al., 2016; McKenzie et al., 2007; Treat et al., 2013)
<b>Mineral soil solid thermal conductivity</b>	<b>1.40 to 1.84 W m<sup>-2</sup> °C<sup>-1</sup></b>	Mean value from (Kurylyk et al., 2016) (1.62 W m <sup>-2</sup> K <sup>-1</sup> ) +/- half of range of organic soil thermal conductivity
Organic soil solid specific heat	1920 J kg <sup>-1</sup>	(McKenzie et al., 2007)
Mineral soil solid specific heat	870 J kg <sup>-1</sup>	(Campbell & Norman, 2000)
Liquid water thermal conductivity	0.6 W m <sup>-2</sup> °C <sup>-1</sup>	(McKenzie & Voss, 2013)
Liquid water specific heat	4182 J kg <sup>-1</sup>	(McKenzie & Voss, 2013)
Ice thermal conductivity	2.13 W m <sup>-2</sup> °C <sup>-1</sup>	(McKenzie & Voss, 2013)
Ice specific heat	2108 J kg <sup>-1</sup>	(McKenzie & Voss, 2013)
<i>Hydrologic Properties</i>		
<b>Organic soil vertical permeability</b>	<b>10<sup>-15</sup> to 10<sup>-10</sup> m<sup>2</sup></b>	Literature values for peat (Jiang et al., 2015b; Naasz et al., 2005; Schwärzel et al., 2006; da Silva et al., 1993; Zhang et al., 2010)
<b>Mineral soil vertical permeability</b>	<b>10<sup>-15</sup> to 10<sup>-11</sup> m<sup>2</sup></b>	(Carsel & Parrish, 1988) mean for silt loam soil +/- 2 orders of magnitude

Vertical/Horizontal Permeability Ratio	0.1	
<b>Organic soil porosity</b>	<b>0.60 to 0.80</b>	Volumetric water content measurements (Rocha et al., 2008a, 2008b, 2008c; Romanovsky et al., 2017)
<b>Mineral soil porosity</b>	<b>0.35 to 0.55</b>	(Carsel & Parrish, 1988) mean for silt loam soil +/- 0.10
<i>Soil Freezing Properties</i>		
Soil freezing function	Linear	(McKenzie & Voss, 2013)
Minimum liquid saturation	0.01	(McKenzie & Voss, 2013)
Temperature below which minimum liquid saturation occurs	-2 °C	(McKenzie & Voss, 2013)
Relative permeability function	Linear	(McKenzie & Voss, 2013)
Minimum relative permeability	$1 \times 10^{-8}$	(Kurylyk et al., 2016)

173

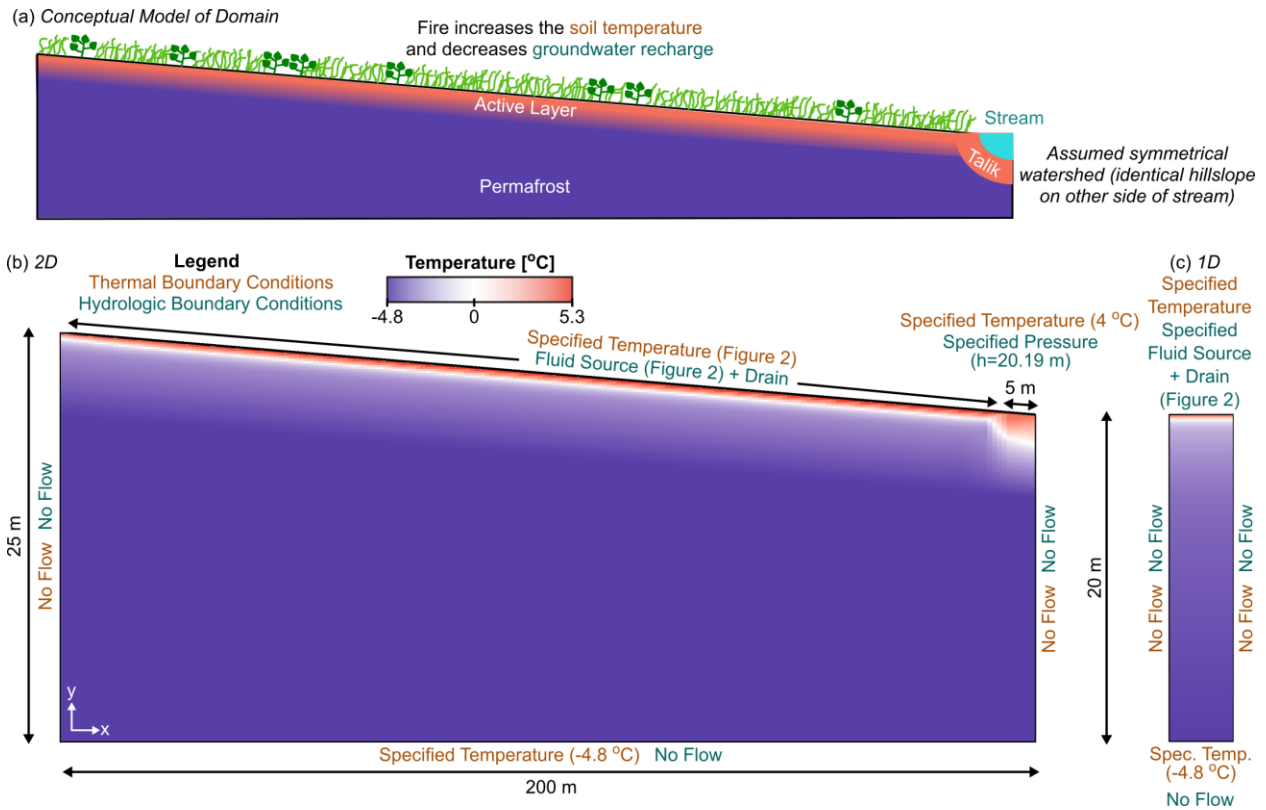
174 *2.2.1 Domain and discretization*

175 We created two separate domains intended to isolate the impact of groundwater flow on  
176 permafrost response to fire: a one-dimensional (1D) vertical column in which no groundwater  
177 flow occurs; and a two-dimensional (2D) watershed cross-section with groundwater flow  
178 induced by a sloping land surface and a stream with an underlying talik at the downstream end of  
179 the domain (Figure 1). The 2D domain represents one half of a symmetric catchment, and  
180 therefore it is not necessary to simulate the image hillslope on the other side of the stream (Evans  
181 et al., 2018; Ge et al., 2011). The archetypal domains are not intended to perfectly recreate the  
182 Anaktuvuk River field sites, but rather to isolate the impact of groundwater along the dominant  
183 hydrogeologic flow field (typically perpendicular to groundwater divides such as streams), thus  
184 allowing for a process-based exploration of fire impacts on groundwater-permafrost interactions  
185 (Voss, 2011a, 2011b; Zipper et al., 2018).

186 For both domains, our conceptual model was that of a two-layer (organic soil and mineral  
187 soil), fully saturated subsurface with homogeneous hydrologic and thermal properties within  
188 each layer. The organic soil layer ranged from 0.09 to 0.18 m in thickness depending on the  
189 scenario simulated (Table 2). We discretized the model into 120 vertical layers, increasing in  
190 thickness from 0.03 m at the land surface to 2.0 m at the bottom of the domain. The 2D domain  
191 was 41 nodes (40 elements) wide, with a uniform node spacing of 5 m. We tested this spacing to  
192 ensure modeled thaw depth was minimally sensitive to the discretization (Figure S2). The land  
193 surface of the 2D domain sloped from 25 m (at x=0 m) to 20 m (at x=200 m), to produce a 2.5%  
194 slope typical of the ARF region (Rocha & Shaver, 2011b). At the right edge of the 2D domain,

195 we used a boundary condition representative of a simplified stream with underlying talik (see  
 196 Section 2.2.2).

197



198

199 **Figure 1.** (a) Conceptual model of domain indicating active layer underlain by permafrost with stream  
 200 and talik along right edge (not to scale). Model domain for (a) 2D domain, which includes lateral  
 201 groundwater flow; and (b) 1D domain, which ignores lateral groundwater flow. Colors in (b) and (c) show  
 202 simulated temperature for unburned (UB) site on September 1, 2009.

203

204 In total, we constructed six unique model domains based on a factorial combination of  
 205 model dimensionality (1D and 2D) and burn severity (UB, MB, and SB), which differed in the  
 206 relative thickness of the organic and mineral soil layers (Table 2). In the following sections, we  
 207 describe the boundary conditions (Section 2.2.2) which were applied to each domain to explore  
 208 parameter sensitivity (Section 2.2.3) and separate the impacts of changes in the water and energy  
 209 balances (Section 2.3).

209



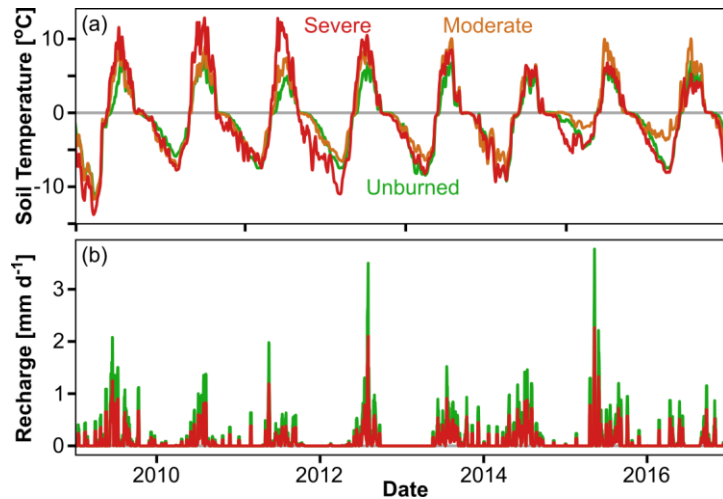
210 **Table 2.** Scenarios simulated.

<b>Scenario</b>	<b>Purpose</b>	<b>Recharge Input</b>	<b>Temperature Input</b>	<b>Organic Layer Thickness [m]</b>
Unburned [UB]	Model calibration	Unburned ARF site	Unburned ARF site	0.18
Moderate Burn [MB]	Model validation	Moderate burn ARF site	Moderate burn ARF site	0.12
Severe Burn [SB]	Model calibration	Severe burn ARF site	Severe burn ARF site	0.09
Severe-Recharge Change Only [SB <sub>w</sub> ]	Isolate water balance change effects	Severe burn ARF site	Unburned ARF site	0.09
Severe-Temperature Change Only [SB <sub>E</sub> ]	Isolate energy balance change effects	Unburned ARF site	Severe burn ARF site	0.09

211

212 *2.2.2 Inputs and boundary conditions*

213 Model thermal and hydrologic boundary conditions for each domain were temporally  
214 constant on the bottom, left, and right sides (Figure 1). While specified heat flux bottom  
215 boundary conditions are often used for studies of permafrost-groundwater interactions (Evans &  
216 Ge, 2017; Kurylyk et al., 2016; McKenzie & Voss, 2013; Wellman et al., 2013), the focus of our  
217 study was exclusively shallow processes occurring in the active layer occurring on a decadal  
218 timescale. Therefore, we decided to use a specified temperature bottom boundary condition at  
219 the zero annual temperature amplitude depth to reduce the size of the model domain and permit a  
220 more detailed sensitivity analysis (Section 2.2.3). We defined this temperature (-4.8 °C) and  
221 bottom boundary depth (20 m) based on ground temperature measurements at the Seabee  
222 Borehole (69.38°N, 152.18°W; 87 km from ARF sites), part of the Global Terrestrial Network  
223 for Permafrost database (Clow, 2014). Since the specified temperature is below the temperature  
224 at which minimum liquid saturation occurs, this bottom boundary will always be completely  
225 frozen and was simulated as a no-flow hydrologic boundary. Thermal and hydrologic boundary  
226 conditions on the right and left edges were no-flow based on the assumption of hydrologic  
227 symmetry around the stream at the center of the watershed (Section 2.2.1).



228  
 229 **Figure 2.** Upper boundary conditions applied to groundwater flow model at ARF sites. (a) Soil  
 230 temperature, and (b) groundwater recharge inputs. In (b), severe and moderate inputs are the same.  
 231

232 The upper thermal boundary condition was time-varying daily specified temperature  
 233 based on soil temperature measurements from each of the three burn severity sites (Figure 2a).  
 234 By using subsurface soil temperature as model input, this boundary condition accounts for  
 235 changes to the energy balance at the land surface, e.g. due to changes in albedo, snow insulation,  
 236 and vegetation. From the time of flux tower installation at the ARF sites (June 2008) through the  
 237 end of 2016, we used measured daily soil temperature at 0.05 m depth from each ARF site  
 238 (Figure 2a) (Shaver and Rocha, 2015a-o). For the 2009-2016 period, there were 749, 480, and  
 239 343 days without data at the UB, MB, and SB sites, respectively, which primarily occurred  
 240 during the winter. We gap-filled missing soil temperature data for the post-fire period using  
 241 linear interpolation for gaps up to seven days in length. For gaps greater than seven days, which  
 242 primarily occurred during January-June 2008 (prior to the installation of monitoring equipment),  
 243 we used the average soil temperature for that day of year and burn severity from years where  
 244 data were present.

245 The upper hydrologic boundary condition was a specified daily fluid source to the top  
 246 layer of nodes, representing groundwater recharge (Figure 2b). Groundwater recharge was  
 247 estimated using a set fraction of daily combined rainfall and snowmelt from a temperature-based  
 248 snowpack model (Walter et al., 2005) implemented within the *EcoHydrology* R package (Fuka  
 249 et al., 2014) and driven using daily meteorological data from the Toolik Field Station, which is  
 250 ~40 km from the study sites (Environmental Data Center Team, 2017). Following Evans & Ge  
 251 (2017), we used 20% of combined rainfall and snowmelt as a fluid source for the UB site. At the  
 252 MB and SB sites, we decreased this value by 40% (resulting in a fluid source equal to 12% of  
 253 combined daily rainfall and snowmelt) because flux tower measurements found that annual  
 254 evapotranspiration at the MB and SB sites was consistently ~40-45% higher than the UB site;  
 255 this has been attributed to increased surface water pooling associated with the thinner organic  
 256 layer following fire (Rocha & Shaver, 2011b). Since this increase is consistent over the 2008-

257 2016 period studied, we do not consider healing of the soil organic layer as an important factor in  
258 controlling differences in groundwater recharge. Healing occurs over longer timescales than the  
259 sub-decadal analysis performed here, and these effects are likely smaller than the large  
260 uncertainty in precipitation estimates in tundra settings (Liljedahl et al., 2017). Generalized  
261 pressure (or drain) boundary conditions were also implemented along the top boundary condition  
262 to prevent overpressuring (Evans & Ge, 2017). Therefore, not all of the fluid source provided  
263 will enter the groundwater flow system. For example, when the top nodes were frozen the drain  
264 nodes prevented excess water from entering the domain.

265 In the 2D domain, the rightmost 5 m (2 nodes) of the domain were specified pressure  
266 nodes at the land surface with a hydraulic head corresponding to 20.19 m and specified  
267 temperature of 4 °C, intended to represent a river or streambed with an underlying talik (Figure  
268 1a). This head is equal to the land surface elevation 7.5 m from the edge of the domain, or  
269 halfway between the 2<sup>nd</sup> and 3<sup>rd</sup> nodes from the edge, in order to create a hydraulic gradient  
270 equal to the slope of the land surface at the stream (2.5%). We took outflow from these specified  
271 pressure nodes to represent groundwater discharge to surface water.

272 Initial pressure and temperature conditions for both 1D and 2D simulations were defined  
273 using a sequential spin-up approach. First, we used a steady-state simulation to estimate  
274 reasonable pressure and temperature fields to use as initial conditions for transient simulations.  
275 In the steady-state simulations, the upper hydrologic boundary condition was a specified pressure  
276 of 0 Pa (indicating a water table at the land surface) with a temperature of -8.43 °C (the mean  
277 annual soil temperature at the UB site). Following the steady-state simulations, we conducted a  
278 transient spin-up from 1998-2007 at a daily timestep with time-varying specified temperature  
279 and fluid source upper boundary conditions to allow the system to equilibrate to pre-fire  
280 conditions. During the 1998-2007 spin-up period prior to the installation of monitoring  
281 equipment at the ARF, we defined the upper thermal boundary conditions using daily soil  
282 temperature measurements at 0.087 m depth from the Toolik Soil Climate Research Station  
283 (Romanovsky et al., 2017). We then implemented the three different burn severity boundary  
284 conditions for the 2008-2016 period using data from the ARF sites (Figure 2). While post-fire  
285 data were available for the 2008-2016 period, we elected to exclude 2008 results from analysis  
286 because the flux towers were not installed until June 2008.

### 287 *2.2.3 Sensitivity analysis and model evaluation*

288 To examine the sensitivity of modeled active layer thickness to different thermal and  
289 hydrologic parameters under groundwater flow (2D) and no groundwater flow (1D) conditions,  
290 we conducted 5000 simulations while varying parameters using a Latin Hypercube Sample  
291 design (McKay et al., 1979) for each combination of dimensionality (1D and 2D) and the burn  
292 severity endmembers (UB and SB), for 20,000 simulations total. We varied six parameters (bold  
293 values in Table 1) representing both hydrological and thermal characteristics of the subsurface:  
294 permeability, thermal conductivity, and porosity of the organic and mineral soil layers. Sampling

295 used a uniform input distribution for each parameter, with permeability log-transformed prior to  
296 sampling.

297 Output from each simulation was daily temperature at each node, which we used to  
298 calculate daily thaw depth for comparison with field observations (Rocha & Shaver, 2015). For  
299 the 2D domain, we used thaw depth from the center of the domain ( $x=100$  m) to minimize  
300 potential edge-effects of the no-flow boundary conditions at the left and right edges of the  
301 domain and the talik at the right edge. As noted in Section 2.2, our modeling approach uses a  
302 simplified domain to isolate key processes of interest (fire-induced changes to the water and  
303 energy balance). Therefore, the comparison with thaw depth measurements is intended to  
304 provide confidence that our model is representing active layer development at the Anaktuvuk  
305 River field site in a reasonable manner, but we are not intending to build a groundwater flow  
306 model specific to each site. Thaw depth is a particularly valuable measurement for model  
307 evaluation in permafrost settings, as it integrates soil temperature through and below the active  
308 layer.

309 For a quantitative metric of model performance, we used the Kling-Gupta Efficiency  
310 (KGE) (Gupta et al., 2009) as implemented in the *hydroGOF* package for R (Zambrano-  
311 Bigiarini, 2014). KGE decomposes the widely-used Nash-Sutcliffe Efficiency (Nash & Sutcliffe,  
312 1970) to provide an overall fit ( $-\infty$  to 1.0) between observed and simulated timeseries, as well as  
313 separate measures of correlation ( $r$ ), bias ( $\beta$ ), and variability ( $\alpha$ ). A value of one corresponds to a  
314 perfect fit for both overall KGE and each decomposed metric. Given that our domain completely  
315 refreezes each winter, the maximum thaw depth for each year is equal to active layer thickness.

316 The relative importance of each parameter to total variability in active layer thickness and  
317 KGE was calculated separately for 1D and 2D cases using a generalized additive model (GAM)  
318 approach, as implemented in the *mgcv* package for R (Wood, 2003, 2011, 2017). GAMs are a  
319 type of generalized linear model integrating smoothing functions which are well-suited for  
320 nonlinear interactions between predictor and response variables. To estimate uncertainty, we  
321 used a bootstrapping approach in which we randomly sampled 75% of the simulation output 100  
322 times to fit GAM models (Serbin et al., 2014; Zipper et al., 2016, 2017b; Zipper & Loheide,  
323 2014). The proportion of variance explained by each parameter for each sample was calculated  
324 as the difference in deviance for a GAM excluding that parameter from the deviance in a GAM  
325 including all parameters, relative to the deviance from a null model.

326 Results from the sensitivity analysis were also used for model calibration and validation.  
327 We selected the parameters with the highest combined KGE between the UB and SB sites in  
328 which KGE at both sites was greater than 0.5. Calibrated model parameters were selected  
329 separately for the 1D and 2D domains. These calibrated parameters were then used to construct  
330 1D and 2D models of the MB site for model validation.

331 

### 2.3 Separating water and energy effects

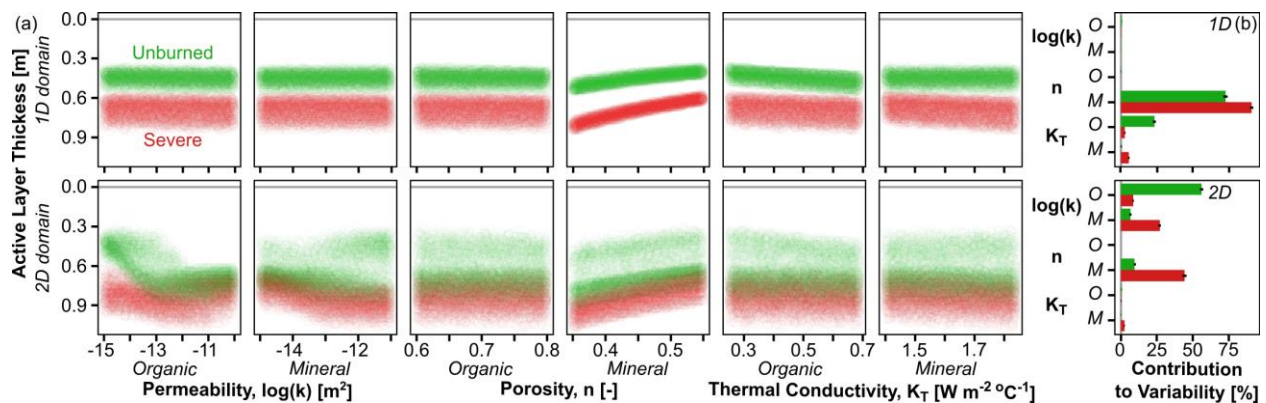
332 To separate the effects of changes to the water and energy balance on permafrost thaw  
 333 and active layer thickness, we conducted two additional simulations on the SB domain (Table 2).  
 334 The first, which is intended to isolate the effects of fire-induced changes in the water balance on  
 335 permafrost thaw, combined recharge from the SB site with soil temperature from the UB site  
 336 (SB<sub>W</sub>). The second was intended to isolate the effects of post-fire changes in the energy balance,  
 337 and combined recharge from the UB site with soil temperature from the SB site (SB<sub>E</sub>).

338 

## 3 Results

339 

### 3.1 Parameter sensitivity analysis



340 **Figure 3.** Sensitivity analysis showing active layer thickness response to thermal and hydrologic  
 341 parameters. (a) Response of active layer thickness (averaged from all post-fire years) to variability in each  
 342 parameter for (top row) 1D and (bottom) 2D domains. Each point represents one simulation from a 5000-  
 343 sample sensitivity analysis. Note that the y-axis is reversed to match the orientation of Figure 1. (b)  
 344 Relative contribution to observed active layer thickness variability for each parameter in (top) 1D and  
 345 (bottom) 2D domains. ‘O’ and ‘M’ labels correspond to Organic and Mineral, respectively, and colors are  
 346 the same as in (a). Bar length is the mean and line shows the minimum/maximum confidence interval  
 347 based on 100-sample bootstrapped analysis. Combined contributions may exceed 100%.  
 348

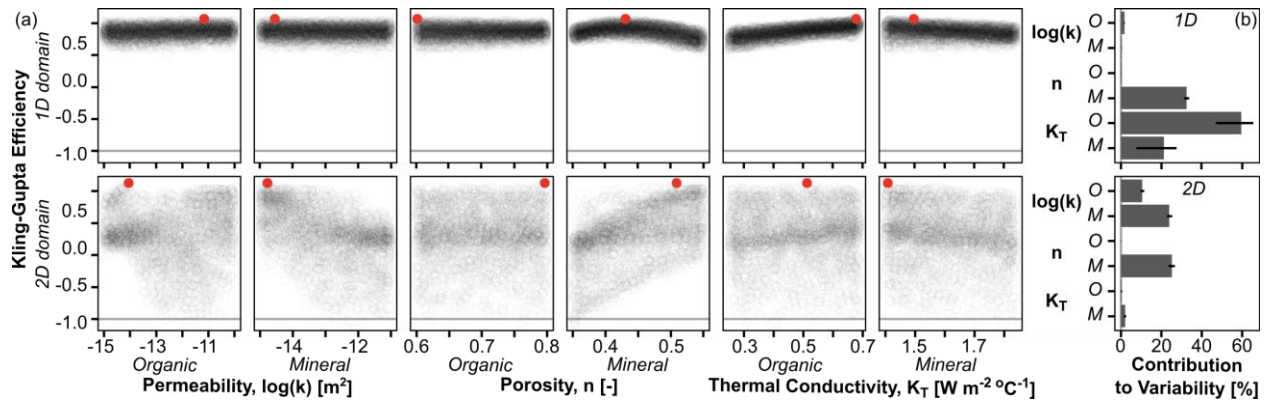
349

350 When groundwater is neglected (1D domain), active layer thickness is most responsive to  
 351 changes in porosity of the mineral soil. There is a strong positive correlation between mean  
 352 annual active layer thickness and porosity, which controls the bulk thermal conductivity of the  
 353 subsurface (Figure 3a, top row). Comparing all parameters, variability in mineral soil porosity  
 354 explains 72.9% (UB) and 90.9% (SB) of variability in active layer thickness (Figure 3b, top  
 355 row). Soil thermal conductivity has a secondary effect on mean annual active layer thickness in  
 356 the 1D simulations, with the relative importance of organic and mineral soil depending on burn  
 357 severity (Figure 3, top row). At the UB site, the solid thermal conductivity of the organic soil  
 358 layer explains 23.5% of variability in active layer thickness, while <1% of variability can be  
 359 attributed to solid thermal conductivity of the mineral soil (Figure 3b, top row). In contrast, at the  
 360 SB site, the relative importance of these two layers is reversed: mineral soil solid thermal

361 conductivity contributes 5.6% of variability in active layer thickness, while organic soil solid  
362 thermal conductivity explains 3.0%. The greater influence of mineral soil properties at the SB  
363 site can be attributed to changes in the thickness of the organic soil layer following fire: the SB  
364 organic layer thickness is 50% that of the UB site (Table 2), thereby decreasing the relative  
365 influence of organic soil properties. The remaining properties evaluated (porosity of the organic  
366 layer, and permeability of both the mineral and organic layers) have a negligible effect on active  
367 layer thickness in the 1D domain (Figure 3, top row).

368 When lateral groundwater flow is simulated (2D domain), modeled sensitivity of the  
369 active layer to hydrologic properties increases, with greatest sensitivity to permeability of the  
370 organic soil in the UB domain, and porosity and permeability of the mineral soil for the SB  
371 domain (Figure 3, bottom row). Permeability of the organic soil layer explains 56.2% (UB) and  
372 8.8% (SB) of variability in active layer thickness and the permeability of the mineral soil layer  
373 contributes 6.8% (UB) and 27.2% (SB) of variability. Active layer thickness is also positively  
374 correlated with mineral soil porosity, which explains 9.7% (UB) and 44.4% (SB) of variability.  
375 The solid thermal conductivity of the mineral soil layer has a tertiary effect on active layer  
376 thickness, explaining 2.7% of variability, while the effects of all other properties are <1%.  
377 Comparing between burn severities, the relative importance of organic soil properties is higher at  
378 the UB site compared to the SB site as in the 1D domain due to the thicker organic layer at the  
379 UB site. There is also greater spread in active layer thickness results for the 2D domain  
380 compared to the 1D domain (Figure 3a), despite the same number of total model parameters,  
381 because thaw depth is sensitive to more parameters when groundwater flow is included (Figure  
382 3b).

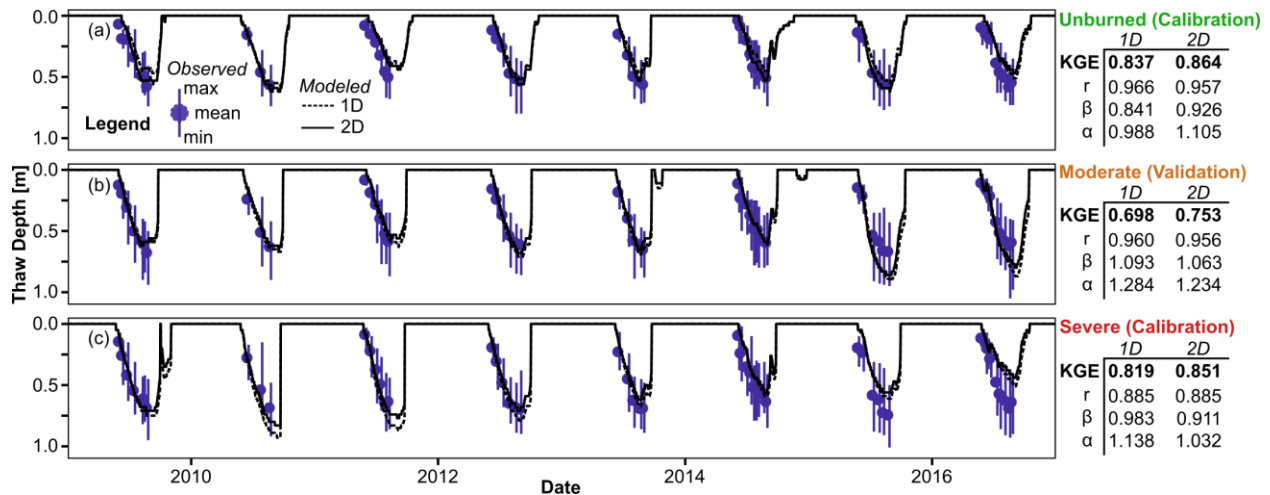
383 The impacts of groundwater on parameter sensitivity is also evident when evaluating  
384 model performance using KGE (Figure 4). In the 1D simulations, KGE is most sensitive to  
385 changes in organic thermal conductivity (59.6% of variability), mineral soil porosity (32.6%),  
386 and mineral soil thermal conductivity (21.3%); all other parameters explain <2% of total  
387 variability in KGE. In the 2D domain, mineral soil porosity and permeability are the dominant  
388 controls (25.2% and 23.7%, respectively), followed by organic permeability (10.8%); all other  
389 parameters explain <2% of variability in KGE. In reality, permeability is related to effective  
390 porosity (Carman, 1937; Kozeny, 1927); therefore, our results shed light on the relative  
391 importance of these two coupled factors.



392  
 393 **Figure 4.** Sensitivity analysis showing model fit to observations as a function of thermal and hydrologic  
 394 properties. (a) Response of mean Kling-Gupta Efficiency (Gupta et al., 2009) to variability in each  
 395 parameter for (top row) 1D and (bottom) 2D domains. Each point represents one simulation from a 5000-  
 396 sample sensitivity analysis. The red points show the calibrated parameters for 1D and 2D domains  
 397 (Section 2.2.3), which are plotted in Figure 4. (b) Relative contribution to observed KGE variability for  
 398 each parameter in (top) 1D and (bottom) 2D domains. ‘O’ and ‘M’ labels correspond to Organic and  
 399 Mineral, respectively, and colors are the same as in (a). Bar length is the mean and line shows the  
 400 minimum/maximum confidence interval based on 100-sample bootstrapped analysis. Combined  
 401 contributions may exceed 100%.

### 402 3.2 Comparison to thaw observations

403 Using the results of the sensitivity analysis, we defined calibrated model parameters for  
 404 the 1D and 2D domains. For each domain, we selected the set of parameters that produced the  
 405 best KGE averaged between the UB and SB sites while exceeding 0.5 at both sites (red dots in  
 406 Figure 4). For some parameters (e.g. thermal conductivity of the organic soil layer in the 2D  
 407 domain), there was a large spread and no trend in the relationship between KGE and the  
 408 parameter; this indicates that the modeled active layer thickness is not sensitive to this parameter.  
 409 We then simulated the MB site as a validation test (Figure 5). Since the response of KGE to both  
 410 mineral soil porosity and permeability is linear with the calibrated parameters near one end, it  
 411 may be argued that increasing the range of variability would better reproduce observations by  
 412 identifying the point at which model performance peaks. However, given that the sampling fully  
 413 encompasses a reasonable range of values for the silt loam soil type observed at the site (Carsel  
 414 & Parrish, 1988; Romanovsky et al., 2017), we elected to not further expand the sensitivity  
 415 analysis to avoid model overfitting.



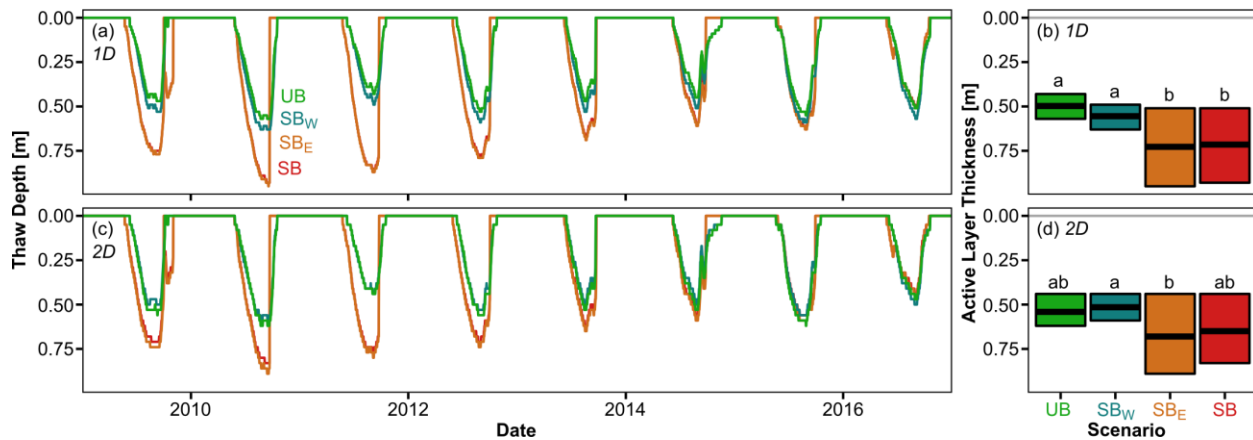
416  
 417 **Figure 5.** Model calibration and validation results for (a) unburned, (b) moderate burn, and (c) severe  
 418 burn sites. Fit statistics are the overall Kling-Gupta Efficiency (KGE), as well as the decomposed KGE  $r$   
 419 (measure of correlation; Pearson coefficient),  $\beta$  (measure of bias; ratio of means of simulated to observed  
 420 values), and  $\alpha$  (measure of variability; ratio of standard deviations of simulated to observed values)  
 421 parameters (Gupta et al., 2009).

422 Overall, both 1D and 2D calibrated models performed well for the calibration and  
 423 validation sites (KGE>0.65; Figure 5). At the SB site, modeled thaw depth was underpredicted in  
 424 later years, particularly 2016. This is associated with a notable decrease in annual soil  
 425 temperature amplitude at the SB site, which behaves similarly to the UB site by the end of the  
 426 simulation period (Figure 2). However, the SB site still has the highest daily soil amplitude (not  
 427 shown), indicating that subdaily thermal dynamics may be a key control on thaw depth not  
 428 included in our modeling approach. Validation performance was weaker for the 1D domain than  
 429 the 2D domain, primarily due to overpredicting thaw depth ( $\beta=1.093$ ) and variability ( $\alpha=1.284$ )  
 430 in the 1D domain. Model performance assessed using KGE is better for the 2D calibrated model  
 431 than the 1D calibrated model at all sites, potentially resulting from lateral groundwater flow in  
 432 the 2D model (Section 3.1).

### 433 3.3 Response to water and energy balance changes

434 Following fire, interannual variability in the active layer thickness and thaw depth  
 435 increased substantially. The four scenarios used to separate water and energy balance effects fall  
 436 into two groups: scenarios with soil temperature inputs from the severe burn site (SB and SB<sub>E</sub>)  
 437 have deeper thaw (Figure 6a,c) and more variability (Figure 6b,d) than scenarios with soil  
 438 temperature from the unburned site (UB and SB<sub>W</sub>). These dynamics are comparable in both the  
 439 absence (1D) and presence (2D) of groundwater flow and indicate that post-fire changes in active  
 440 layer thickness are driven primarily by changes to the energy balance. However, these changes  
 441 are relatively short-lived; by 2014 (seven years after the fire), seasonal patterns of permafrost  
 442 thaw and active layer thickness are comparable across all simulations, as temperature at the UB  
 443 and SB sites are comparable (Figure 2).

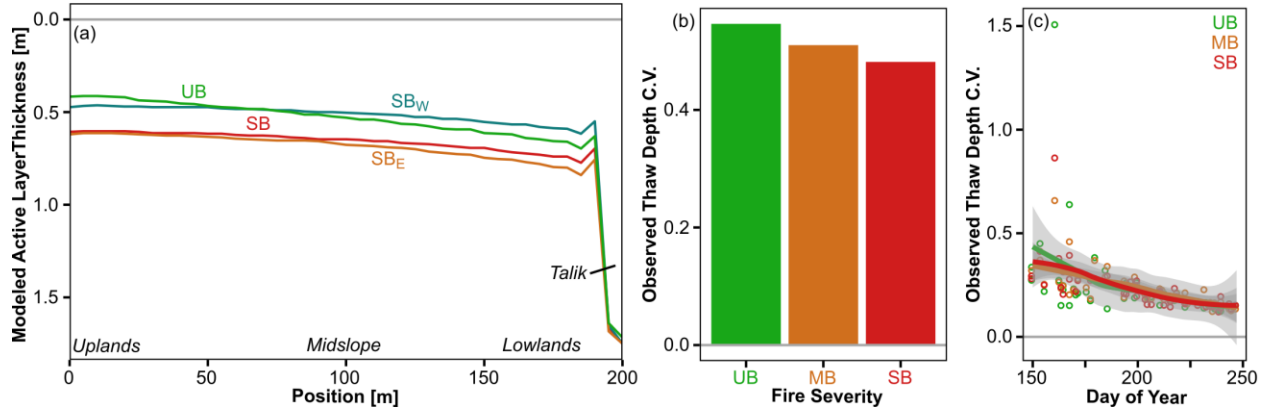




444  
 445 **Figure 6.** Comparison of daily thaw depth for different water and energy balance scenarios showing  
 446 dominant effect of temperature. (a) Timeseries of thaw depth for different scenarios in 1D domain. Names  
 447 correspond to Table 2. (b) Boxplot showing range and mean of active layer thickness for each scenario in  
 448 1D domain. Different letters denote significantly different means ( $p < 0.05$ ) between scenarios, as tested  
 449 using the Tukey Honest Significant Differences test. (c) Thaw depth for different scenarios with 2D  
 450 domain; (d) range and mean of active layer thickness for 2D domain.

451 In contrast, both field measurements and model results indicate that spatial variability in  
 452 thaw depth is highest at the unburned site and decreases as a function of burn severity (Figure 7).  
 453 The coefficient of variation (C.V.) of thaw depth measurements is 13.4% greater at the UB site  
 454 compared to the SB site (0.55 vs 0.48), with MB occupying an intermediate position (Figure 7b).  
 455 Temporal patterns in thaw depth variance are consistent across sites, with the largest C.V. early  
 456 in the summer when mean thaw depth is lowest, and a decreasing C.V. as time goes on (Figure  
 457 7c). Thus, while previous work documented an increase in thaw depth at these sites following  
 458 fire (Rocha & Shaver, 2011b), relative variability in active layer thickness decreases due to fire  
 459 in observed data, consistent with observed decreases in lateral thaw gradients shown in  
 460 simulation results (Figure 7a).

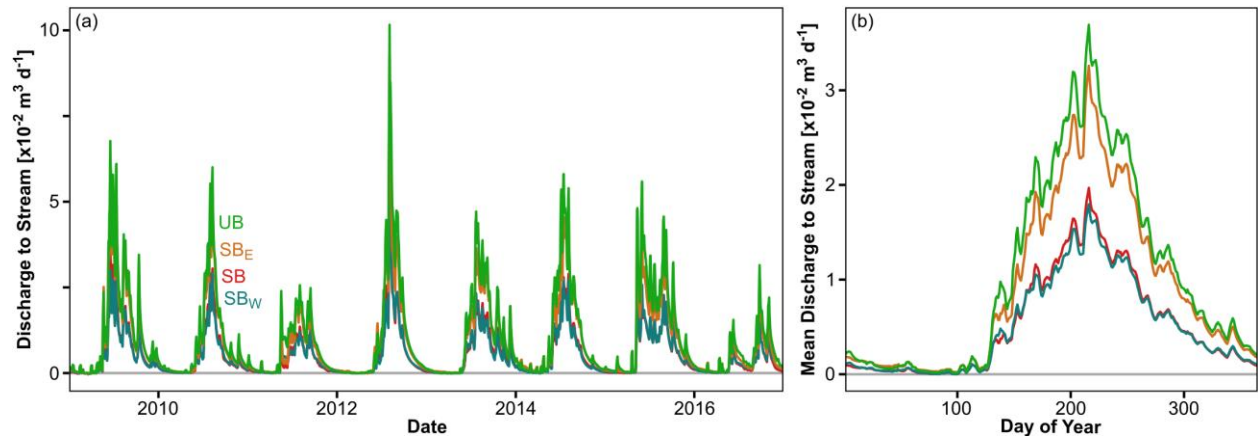
461 Model results indicate that the decreased spatial variability in thaw depth following fire is  
 462 driven by reduced groundwater flow (Figure 7a). In all scenarios including groundwater flow  
 463 (2D domain), permafrost response varies along a gradient, with thinner active layers in the  
 464 upland portion of the domain and thicker active layers in the lowland portion of the domain.  
 465 Lateral thaw depth variability is largest in the scenarios without changes in the water balance due  
 466 to fire: in the UB scenario active layer thickness is 0.24 m greater in the lowland region ( $x=180$   
 467 m) compared to the upland region ( $x=20$  m), a 57% increase, followed by the SB<sub>E</sub> simulation  
 468 (30% increase). Reductions in groundwater recharge due to fire decrease the degree of active  
 469 layer thickness variability over the domain and reduce the difference between uplands and  
 470 lowland regions to 26% in the SB<sub>W</sub> scenario and 23% in the SB scenario.



471  
 472 **Figure 7.** (a) Cross-section of modeled mean annual active layer thickness for each 2D water and energy  
 473 balance scenario (colored lines). Names correspond to Table 2. Italics denote different regions referred to  
 474 in the text. (b) Coefficient of variation (C.V.) for thaw depth observations group by site and day of year  
 475 for 2009-2016. (c) C.V. of thaw depth for each site by day of year across entire 2009-2016 period.

### 476 3.4 Groundwater discharge to surface water features

477 Fire may impact groundwater discharge to surface water features (e.g. rivers and streams)  
 478 by changing both the supply of water (via altered recharge) and the transmissivity of the  
 479 subsurface (via altered active layer thickness). Here, fire led to an approximately 50% reduction  
 480 in the quantity of water released from groundwater to surface water, with mean annual discharge  
 481 decreasing from 3.78 m<sup>3</sup> in the UB scenario to 1.91 m<sup>3</sup> in the SB scenario (Figure 8), which is  
 482 greater than the prescribed 40% decrease in groundwater recharge to the model (Figure 2). This  
 483 decrease is due primarily to reduced groundwater recharge following fire: the lowest observed  
 484 mean annual discharge (1.83 m<sup>3</sup>) occurs in the SB<sub>W</sub> scenario, when only groundwater recharge  
 485 changes, while there is a slight reduction in mean annual discharge when only soil temperature  
 486 changes (3.26 m<sup>3</sup> in the SB<sub>E</sub> scenario). However, there was no observed shift in the timing of  
 487 groundwater discharge to streams in either the onset of groundwater discharge in the spring or  
 488 the day of peak discharge, despite the observed changes in the timing and magnitude of thaw  
 489 between the different burn severities which controls groundwater recharge and flow in the  
 490 subsurface (Figure 6).



492 **Figure 8.** Discharge at specified pressure nodes representing stream for each 2D water and energy  
493 balance scenario (colored lines) for (a) entire 2009-2016 period; and (b) average for each day of year.  
494 Names correspond to Table 2.

## 495 **4 Discussion**

### 496 *4.1 Importance of groundwater flow*

497 Three lines of evidence support out hypothesis that heat transport via groundwater flow is  
498 a key control over permafrost response to fire. First, for a given set of parameters, active layer  
499 thickness is greater in simulations including groundwater flow (2D domain) compared to  
500 simulations neglecting groundwater flow (1D domain), indicating that heat transport via  
501 advection enhances permafrost thaw relative to conduction-dominated simulations (Figures 3 and  
502 4). Second, including groundwater flow increases the relative importance of hydraulic properties  
503 (soil permeability) and decreases the relative importance of thermal properties (soil thermal  
504 conductivity), indicating that subsurface heat transport by advection is of greater importance than  
505 heat transport by conduction (Figures 3 and 4). Third, model calibration and validation  
506 performance is better in the 2D simulations where groundwater flow is included compared to the  
507 1D simulations where groundwater flow is ignored (Figure 5), indicating that including  
508 groundwater flow is a more accurate representation of real-world conditions. Combined, these  
509 results indicate that lateral heat transport through the active layer via groundwater flow is an  
510 important but underappreciated component of post-fire permafrost dynamics, and the relative  
511 importance of advective heat transport will likely be greater where groundwater flow rates are  
512 higher (e.g. more conductive sediments or a higher hydraulic gradient).

513 While previous work has shown that heat transport via lateral groundwater flow can be a  
514 positive feedback to permafrost degradation (e.g. Bense et al., 2009, 2012; Connon et al., 2018,  
515 2014; Kurylyk et al., 2016), this is the first study to demonstrate that advective heat transport is a  
516 key driver of the permafrost response to fire. Importantly, it suggests that spatial variability in  
517 the ecohydrological response to fire, a key research priority for disturbance hydrology (Mirus et  
518 al., 2017), may be in part driven by groundwater flow which enhances permafrost degradation in  
519 lowland areas (Figure 7). Based on our results, we suggest that the degree to which fire effects  
520 can be transported laterally via groundwater flow are strongly dependent on post-fire hydraulic  
521 gradients and soil properties. Given that both the vertical water balance and soil hydraulic  
522 properties may be modified by fire (Kettridge et al., 2012, 2017; Lukenbach et al., 2016;  
523 Semenova et al., 2015; Sherwood et al., 2013; Thompson et al., 2014; Thompson & Waddington,  
524 2013), this represents a potential post-fire feedback which merits further investigation. For  
525 example, since deeper organic soils are often less conductive than near-surface organic soils,  
526 burning off the near-surface soil would lead to a decrease in the average hydraulic conductivity  
527 of the organic soil layer (Hinzman et al., 1991; Quinton et al., 2008).

#### 528 4.2 Active layer thickness response to water and energy balance changes

529 We also demonstrate that changes to the water and energy balance have opposite effects  
530 on permafrost thaw depth. Changes to the energy balance increase both conductive and advective  
531 energy transport into the subsurface by increasing near-surface soil temperatures which act as an  
532 upper boundary to the system (Figure 2), leading to an increase in active layer thickness in both  
533 SB and SB<sub>E</sub> scenarios relative to the UB scenario (Figure 6). In contrast, changes to the water  
534 balance lead to a reduction in groundwater recharge, which reduces advective heat transport and  
535 decreases active layer thickness in the SB<sub>W</sub> scenario relative to the UB scenario (Figure 6).

536 Our results indicate that changes to the energy balance are the dominant control over the  
537 thickness of the active layer following fire as evidenced by the similarity in thaw depth between  
538 simulations for the SB site and simulations with only changes to the energy balance (SB<sub>E</sub>)  
539 (Figure 6, 7). While the dominance of energy balance changes may seem to contradict the strong  
540 sensitivity of modeled thaw dynamics to hydrological parameters (Figures 3 and 4), these results  
541 are reconciled by noting that heat transport via advection is a function of both the energy content  
542 of groundwater (a function of soil temperature) and the magnitude of groundwater flow (a  
543 function of recharge and active layer thickness). Therefore, changes in the energy balance can be  
544 the dominant driver of permafrost thaw dynamics as observed in previous studies (Brown et al.,  
545 2016), even where groundwater flow is an important process. As warming in high-latitude  
546 regions shifts the timing and magnitude of spring snowmelt, changes in to the water balance may  
547 increase in importance (Bring et al., 2016; Lique et al., 2016), in particular at sites with finer-  
548 grained mineral soils which are able to hold more unfrozen water even at subzero temperatures,  
549 buffering permafrost from changes in air temperature (Nicolosky & Romanovsky, 2018).

550 In contrast, changes to the water balance are the dominant control over spatial variability  
551 in active layer thickness as evidenced by greater lateral heterogeneity in active layer thickness in  
552 simulations with higher groundwater recharge rates (UB, SB<sub>E</sub>) (Figure 7). This variability is not  
553 random, but a function of landscape position with greater differences in active layer thickness  
554 between uplands (less thaw) and lowlands (more thaw) in simulations in which there is more  
555 groundwater flow. This is consistent with field observations showing a decrease in the relative  
556 variability of thaw depth following fire (Figure 7b-c). While our study focused on a continuous  
557 permafrost environment, thaw in lowland areas may be particularly important in areas of  
558 discontinuous permafrost where it is likely to increase subsurface hydrologic connectivity which  
559 can induce ecologically significant land cover transitions (Connon et al., 2014; Kurylyk et al.,  
560 2016; Quinton et al., 2011).

#### 561 4.3 Baseflow response to water and energy balance changes

562 We show that the supply of water (groundwater recharge) is the key control over post-fire  
563 changes in baseflow (Figure 8), leading to up to ~50% decreases in annual groundwater  
564 discharge in the SB and SB<sub>W</sub> scenarios. Changes in transmissivity appear to have little effect, as  
565 the SB<sub>E</sub> scenario which had the largest increase in active layer thickness (Figures 6, 7) has a

566 negligible change in groundwater discharge to the stream under the conditions simulated (Figure  
567 8). Changes in recharge alone are not sufficient to explain the simulated 50% decreases in  
568 groundwater discharge, as fire led to only a 40% reduction in groundwater recharge (Figure 2).  
569 Therefore, we suggest that a weakening of the hydraulic gradient following fire, caused by a  
570 reduction in groundwater recharge and advective heat transport leading to smaller differences in  
571 active layer thickness between upslope and downslope portions of the domain (Figure 7a), may  
572 also be an important driver of changes in baseflow following fire.

573 Relatively little work has examined changes in groundwater-surface water interactions  
574 following fire in permafrost environments. In Alaska, post-fire flow during rain events was  
575 enhanced by the increased thickness of the active layer (Petronne et al., 2007). While our study  
576 does not examine response to individual precipitation events, the observed increases in active  
577 layer thickness resulting from fire (e.g. Figure 7a) provides a mechanism for these increases in  
578 stormflow by providing more space in the near-surface soil layers through which water can flow.  
579 In contrast, in our simulations lower water inputs led to a net decrease in groundwater discharge  
580 to streams. At larger scales, previous work has shown that forest fires cause a slight increase in  
581 streamflow in Arctic settings, though this signal is small relative to changes in atmospheric  
582 moisture transport (McClelland et al., 2004).

583 We suggest that the impacts of fire on groundwater discharge to streams depend strongly  
584 on local site characteristics, given the substantial uncertainty regarding post-fire changes to the  
585 water and energy balance. For instance, previous work has demonstrated that in settings where  
586 permafrost thaw leads to enhanced subsurface connectivity (e.g. the talik grows deep enough to  
587 connect to a subpermafrost aquifer), groundwater flow processes can exert a major control  
588 (Bense et al., 2012). Thus, the impacts of fire on baseflow may be stronger in regions of  
589 discontinuous permafrost with more dynamic changes in hydrologic connectivity (Connon et al.,  
590 2014, 2015; Walvoord et al., 2012). Furthermore, at our study site fire was associated with an  
591 increase in evapotranspiration and concomitant reduction in groundwater recharge (Rocha &  
592 Shaver, 2011b); work elsewhere has documented both increases (Thompson et al., 2014) and  
593 decreases (Liu et al., 2005) in evapotranspiration following fire in cold regions, indicating that  
594 advances to our understanding of the land surface water and energy balance are necessary to  
595 improve boundary representation in subsurface models.

#### 596 *4.4 Study limitations*

597 Despite the strong model performance when compared to field observations (Figure 5),  
598 there are several limitations to our approach which may affect our results. First, freeze/thaw  
599 processes in our model only consider freezing of water within existing pore space, and therefore  
600 processes such as thermokarst development and ice lensing are not simulated. Second, our  
601 archetypal modeling approach simulates saturated flow with homogeneous subsurface properties;  
602 variably saturated processes may be important, particularly in high-porosity soils in which air-  
603 filled pore space can act as a thermal buffer (Kettridge et al., 2012; Quinton et al., 2000). Since  
604 our upper thermal boundary condition is based on soil temperature measurements at a depth of 5

605 cm, it accounts for near-surface drying but may be inaccurate if the water table falls below the  
606 soil temperature sensor which would likely occur in late summer. Previous work in the ARF  
607 region found that the mineral soil layer tends to stay saturated, while the organic layer dries  
608 seasonally (Hinzman et al., 1991). Therefore, if we considered variably saturated conditions, the  
609 sensitivity of our results to the porosity of the organic layer may increase, as porosity is the main  
610 control over the potential amount of air-filled pore space. The relative importance of vertical heat  
611 transport would decrease due to reduced conduction through air-filled pore space, thus further  
612 supporting our argument that lateral groundwater flow is a critical but often ignored part of the  
613 permafrost response to fire.

614 Third, our model is only of the subsurface, and therefore does not simulate ponding at the  
615 land surface which may occur during snowmelt or precipitation events if there is insufficient  
616 infiltration capacity; this limitation likely reduces both the quantity and duration of groundwater  
617 recharge, particularly during spring snowmelt, and may dampen effects of changes in the water  
618 balance. Finally, our specified boundary condition intended to represent a streambed is  
619 simplified and does not include temporal dynamics (e.g. high water levels during spring freshet,  
620 seasonal changes in temperature) which may influence stream-aquifer interactions. Additional  
621 field measurements such as stream stage, stream temperature, and water table gradient in the  
622 hillslope areas may help resolve some of these uncertainties and aid in the construction of a site-  
623 specific model.

624 While our modeling approach may neglect some locally-important processes, the  
625 objective of our research was to isolate the effects of groundwater flow on post-fire permafrost  
626 distribution. Our archetypal approach to groundwater modeling provides information about the  
627 fundamental processes controlling system dynamics, and therefore provides more generalizable  
628 information than highly parameterized models. By making these assumptions, we are better able  
629 to isolate the role of groundwater, providing a more generalized understanding of flow processes  
630 in variably frozen porous media, which physical properties and model parameters most strongly  
631 influence the response of subsurface processes to fire, and how fire-induced changes are able to  
632 propagate laterally through groundwater flow.

## 633 **5 Conclusions**

634 In this study, we quantified the importance of groundwater flow to permafrost thaw following  
635 fire. Our results demonstrate that hydrogeological processes are a key control over permafrost  
636 dynamics following fire, and that neglecting lateral water and heat transport may lead to  
637 overestimation of the importance of thermal properties. We also show that an increase in energy  
638 input to the subsurface following fire is the primary driver of increases in active layer thickness,  
639 and permafrost thaw is enhanced by advective heat transport via groundwater flow. However,  
640 changes to the water balance are the key control over post-fire spatial heterogeneity in thaw  
641 depth and groundwater discharge to surface water features. These results show that groundwater  
642 flow and associated processes must be considered to understand both terrestrial and hydrological  
643 response to fire in permafrost settings.

644 **Acknowledgments and Data**

645 SCZ, PLH, and JMM were funded by the Natural Sciences and Engineering Research Council of  
 646 Canada (NSERC) and the McGill University Trotter Institute for Science and Public Policy.  
 647 AVR and data collection were funded by NSF grant #1556772 to the University of Notre Dame.  
 648 We appreciate discussions with Tom Gleeson, Yueyang Jiang, and Barret Kurylyk. Anaktuvuk  
 649 River data sets were provided by the Arctic LTER (Rocha and Shaver, 2015; Shaver and Rocha,  
 650 2015a-o). This material is based upon work supported by the National Science Foundation under  
 651 grants #DEB-981022, 9211775, 8702328; #OPP-9911278, 9911681, 9732281, 9615411,  
 652 9615563, 9615942, 9615949, 9400722, 9415411, 9318529; #BSR 9019055, 8806635, 8507493.  
 653 Meteorological datasets were provided by the Toolik Field Station Environmental Data Center  
 654 (Environmental Data Center Team, 2017) based upon work supported by the National Science  
 655 Foundation under grants #455541 and 1048361. All analyses were performed using R 3.4.0 (R  
 656 Core Team, 2017) and graphics made using ggplot2 (Wickham, 2009) and InkScape (The  
 657 Inkscape Team, 2015). Field data, model input files, and analysis scripts will be made available  
 658 on FigShare at article acceptance.

659 **References**

- 660 Abbott, B. W., Jones, J. B., Schuur, E. A. G., III, F. S. C., Bowden, W. B., Bret-Harte, M. S., ... Zimov, S. (2016).  
 661 Biomass offsets little or none of permafrost carbon release from soils, streams, and wildfire: an expert  
 662 assessment. *Environmental Research Letters*, *11*(3), 034014. <https://doi.org/10.1088/1748-9326/11/3/034014>  
 663 Balshi, M. S., McGuire, A. D., Zhuang, Q., Melillo, J., Kicklighter, D. W., Kasischke, E., ... Shvidenko, A. (2007).  
 664 The role of historical fire disturbance in the carbon dynamics of the pan-boreal region: A process-based  
 665 analysis. *Journal of Geophysical Research-Biogeosciences*, *112*(G2), G02029.  
 666 <https://doi.org/10.1029/2006JG000380>  
 667 Bense, V. F., Ferguson, G., & Kooi, H. (2009). Evolution of shallow groundwater flow systems in areas of  
 668 degrading permafrost. *Geophysical Research Letters*, *36*(22), L22401. <https://doi.org/10.1029/2009GL039225>  
 669 Bense, V. F., Kooi, H., Ferguson, G., & Read, T. (2012). Permafrost degradation as a control on hydrogeological  
 670 regime shifts in a warming climate. *Journal of Geophysical Research-Earth Surface*, *117*, F03036.  
 671 <https://doi.org/10.1029/2011JF002143>  
 672 Bret-Harte, M. S., Mack, M. C., Shaver, G. R., Huebner, D. C., Johnston, M., Mojica, C. A., ... Reiskind, J. A.  
 673 (2013). The response of Arctic vegetation and soils following an unusually severe tundra fire. *Philosophical*  
 674 *Transactions of the Royal Society B-Biological Sciences*, *368*(1624), UNSP 20120490.  
 675 <https://doi.org/10.1098/rstb.2012.0490>  
 676 Bring, A., Fedorova, I., Dibike, Y., Hinzman, L., Mard, J., Mernild, S. H., ... Woo, M.-K. (2016). Arctic terrestrial  
 677 hydrology: A synthesis of processes, regional effects, and research challenges. *Journal of Geophysical*  
 678 *Research-Biogeosciences*, *121*(3), 621–649. <https://doi.org/10.1002/2015JG003131>  
 679 Brooks, R. H., & Corey, A. T. (1964). *Hydraulic properties of porous media* (Hydrology Papers No. 3). Fort  
 680 Collins: Colorado State University.  
 681 Brown, D. R. N., Jorgenson, M. T., Kielland, K., Verbyla, D. L., Prakash, A., & Koch, J. C. (2016). Landscape  
 682 Effects of Wildfire on Permafrost Distribution in Interior Alaska Derived from Remote Sensing. *Remote*  
 683 *Sensing*, *8*(8), 654. <https://doi.org/10.3390/rs8080654>  
 684 Brown, D. R. N., Jorgenson, M. T., Douglas, T. A., Romanovsky, V. E., Kielland, K., Hiemstra, C., ... Ruess, R. W.  
 685 (2015). Interactive effects of wildfire and climate on permafrost degradation in Alaskan lowland forests.  
 686 *Journal of Geophysical Research-Biogeosciences*, *120*(8), 1619–1637. <https://doi.org/10.1002/2015JG003033>  
 687 Campbell, G. S., & Norman, J. M. (2000). *An Introduction to Environmental Biophysics* (2nd ed.). Springer.

- 688 Carman, P. C. (1937). Fluid flow through granular beds. *Trans. Inst. Chem. Eng.*, *15*, 150–166.
- 689 Carsel, R. F., & Parrish, R. S. (1988). Developing joint probability-distributions of soil-water retention  
690 characteristics. *Water Resources Research*, *24*(5), 755–769. <https://doi.org/10.1029/WR024i005p00755>
- 691 Chipman, M. L., & Hu, F. S. (2017). Linkages Among Climate, Fire, and Thermoerosion in Alaskan Tundra Over  
692 the Past Three Millennia. *Journal of Geophysical Research: Biogeosciences*, *122*(12), 3362–3377.  
693 <https://doi.org/10.1002/2017JG004027>
- 694 Clapp, R. B., & Hornberger, G. M. (1978). Empirical equations for some soil hydraulic properties. *Water Resources*  
695 *Research*, *14*(4), 601–604. <https://doi.org/10.1029/WR014i004p00601>
- 696 Clow, G. D. (2014). Global Terrestrial Network for Permafrost - Seabee. Retrieved February 27, 2017, from  
697 <http://gtnpdatabase.org/boreholes/view/812>
- 698 Connon, R. F., Quinton, W. L., Craig, J. R., & Hayashi, M. (2014). Changing hydrologic connectivity due to  
699 permafrost thaw in the lower Liard River valley, NWT, Canada. *Hydrological Processes*, *28*(14), 4163–4178.  
700 <https://doi.org/10.1002/hyp.10206>
- 701 Connon, R. F., Quinton, W. L., Craig, J. R., Hanisch, J., & Sonnentag, O. (2015). The hydrology of interconnected  
702 bog complexes in discontinuous permafrost terrains. *Hydrological Processes*, *29*(18), 3831–3847.  
703 <https://doi.org/10.1002/hyp.10604>
- 704 Connon, R., Devoie, É., Hayashi, M., Veness, T., & Quinton, W. (2018). The Influence of Shallow Taliks on  
705 Permafrost Thaw and Active Layer Dynamics in Subarctic Canada. *Journal of Geophysical Research: Earth*  
706 *Surface*, *123*(2), 281–297. <https://doi.org/10.1002/2017JF004469>
- 707 De Baets, S., van de Weg, M. J., Lewis, R., Steinberg, N., Meersmans, J., Quine, T. A., ... Hartley, I. P. (2016).  
708 Investigating the controls on soil organic matter decomposition in tussock tundra soil and permafrost after fire.  
709 *Soil Biology and Biochemistry*, *99*, 108–116. <https://doi.org/10.1016/j.soilbio.2016.04.020>
- 710 Environmental Data Center Team. (2017). Meteorological Monitoring program at Toolik, Alaska. Toolik Field  
711 Station, Institute of Arctic Biology, University of Alaska Fairbanks, Fairbanks, AK 99775. Retrieved March 27,  
712 2017, from [http://toolik.alaska.edu/edc/abiotic\\_monitoring/data\\_query.php](http://toolik.alaska.edu/edc/abiotic_monitoring/data_query.php)
- 713 Evans, S. G., & Ge, S. (2017). Contrasting hydrogeologic responses to warming in permafrost and seasonally frozen  
714 ground hillslopes. *Geophysical Research Letters*, *44*(4), 2016GL072009.  
715 <https://doi.org/10.1002/2016GL072009>
- 716 Evans, S. G., Ge, S., Voss, C. I., & Molotch, N. P. (2018). The Role of Frozen Soil in Groundwater Discharge  
717 Predictions for Warming Alpine Watersheds. *Water Resources Research*, *54*(3), 1599–1615.  
718 <https://doi.org/10.1002/2017WR022098>
- 719 Flannigan, M. D., Logan, K. A., Amiro, B. D., Skinner, W. R., & Stocks, B. J. (2005). Future area burned in  
720 Canada. *Climatic Change*, *72*(1–2), 1–16. <https://doi.org/10.1007/s10584-005-5935-y>
- 721 Fuka, D., Walter, M., Archibald, J., Steenhuis, J., & Easton, Z. (2014). EcoHydRology: A community modeling  
722 foundation for Eco-Hydrology (Version 0.4.12). Retrieved from [https://CRAN.R-](https://CRAN.R-project.org/package=EcoHydRology)  
723 [project.org/package=EcoHydRology](https://CRAN.R-project.org/package=EcoHydRology)
- 724 Ge, S., McKenzie, J., Voss, C., & Wu, Q. (2011). Exchange of groundwater and surface-water mediated by  
725 permafrost response to seasonal and long term air temperature variation. *Geophysical Research Letters*, *38*(14),  
726 L14402. <https://doi.org/10.1029/2011GL047911>
- 727 Gupta, H. V., Kling, H., Yilmaz, K. K., & Martinez, G. F. (2009). Decomposition of the mean squared error and  
728 NSE performance criteria: Implications for improving hydrological modelling. *Journal of Hydrology*, *377*(1),  
729 80–91. <https://doi.org/10.1016/j.jhydrol.2009.08.003>
- 730 Higuera, P. E., Brubaker, L. B., Anderson, P. M., Brown, T. A., Kennedy, A. T., & Hu, F. S. (2008). Frequent Fires  
731 in Ancient Shrub Tundra: Implications of Paleorecords for Arctic Environmental Change. *PLoS ONE*, *3*(3),  
732 e0001744. <https://doi.org/10.1371/journal.pone.0001744>
- 733 Hinzman, L. D., Kane, D. L., Gieck, R. E., & Everett, K. R. (1991). Hydrologic and thermal properties of the active  
734 layer in the Alaskan Arctic. *Cold Regions Science and Technology*, *19*(2), 95–110.  
735 [https://doi.org/10.1016/0165-232X\(91\)90001-W](https://doi.org/10.1016/0165-232X(91)90001-W)



- 736 Hu, F. S., Higuera, P. E., Walsh, J. E., Chapman, W. L., Duffy, P. A., Brubaker, L. B., & Chipman, M. L. (2010).  
737 Tundra burning in Alaska: Linkages to climatic change and sea ice retreat. *Journal of Geophysical Research:*  
738 *Biogeosciences*, 115(G4), G04002. <https://doi.org/10.1029/2009JG001270>
- 739 Hu, F. S., Higuera, P. E., Duffy, P., Chipman, M. L., Rocha, A. V., Young, A. M., ... Dietze, M. C. (2015). Arctic  
740 tundra fires: natural variability and responses to climate change. *Frontiers in Ecology and the Environment*,  
741 13(7), 369–377. <https://doi.org/10.1890/150063>
- 742 Iwahana, G., Harada, K., Uchida, M., Tsuyuzaki, S., Saito, K., Narita, K., ... Hinzman, L. D. (2016).  
743 Geomorphological and geochemistry changes in permafrost after the 2002 tundra wildfire in Kougarak, Seward  
744 Peninsula, Alaska. *Journal of Geophysical Research: Earth Surface*, 121(9), 2016JF003921.  
745 <https://doi.org/10.1002/2016JF003921>
- 746 Jafarov, E. E., Romanovsky, V. E., Genet, H., McGuire, A. D., & Marchenko, S. S. (2013). The effects of fire on the  
747 thermal stability of permafrost in lowland and upland black spruce forests of interior Alaska in a changing  
748 climate. *Environmental Research Letters*, 8(3), 035030. <https://doi.org/10.1088/1748-9326/8/3/035030>
- 749 Jiang, Y., Rastetter, E. B., Shaver, G. R., Rocha, A. V., Zhuang, Q., & Kwiatkowski, B. L. (2017). Modeling long-  
750 term changes in tundra carbon balance following wildfire, climate change, and potential nutrient addition.  
751 *Ecological Applications*, 27(1), 105–117. <https://doi.org/10.1002/eap.1413>
- 752 Jiang, Y., Zhuang, Q., & O'Donnell, J. A. (2012). Modeling thermal dynamics of active layer soils and near-surface  
753 permafrost using a fully coupled water and heat transport model. *Journal of Geophysical Research:*  
754 *Atmospheres*, 117(D11), D11110. <https://doi.org/10.1029/2012JD017512>
- 755 Jiang, Y., Rastetter, E. B., Rocha, A. V., Pearce, A. R., Kwiatkowski, B. L., & Shaver, G. . . (2015a). Modeling  
756 carbon–nutrient interactions during the early recovery of tundra after fire. *Ecological Applications*, 25(6), 1640–  
757 1652. <https://doi.org/10.1890/14-1921.1>
- 758 Jiang, Y., Rocha, A. V., O'Donnell, J. A., Drysdale, J. A., Rastetter, E. B., Shaver, G. R., & Zhuang, Q. (2015b).  
759 Contrasting soil thermal responses to fire in Alaskan tundra and boreal forest. *Journal of Geophysical Research-*  
760 *Earth Surface*, 120(2), 363–378. <https://doi.org/10.1002/2014JF003180>
- 761 Jones, B. M., Kolden, C. A., Jandt, R., Abatzoglou, J. T., Urban, F., & Arp, C. D. (2009). Fire Behavior, Weather,  
762 and Burn Severity of the 2007 Anaktuvuk River Tundra Fire, North Slope, Alaska. *Arctic, Antarctic, and Alpine*  
763 *Research*, 41(3), 309–316. <https://doi.org/10.1657/1938-4246-41.3.309>
- 764 Jones, B. M., Grosse, G., Arp, C. D., Miller, E., Liu, L., Hayes, D. J., & Larsen, C. F. (2015). Recent Arctic tundra  
765 fire initiates widespread thermokarst development. *Scientific Reports*, 5, 15865.  
766 <https://doi.org/10.1038/srep15865>
- 767 Kasischke, E. S., & Johnstone, J. F. (2005). Variation in postfire organic layer thickness in a black spruce forest  
768 complex in interior Alaska and its effects on soil temperature and moisture. *Canadian Journal of Forest*  
769 *Research-Revue Canadienne De Recherche Forestiere*, 35(9), 2164–2177. <https://doi.org/10.1139/X05-159>
- 770 Kasischke, E. S., Bourgeau-Chavez, L. L., & Johnstone, J. F. (2007). Assessing spatial and temporal variations in  
771 surface soil moisture in fire-disturbed black spruce forests in Interior Alaska using spaceborne synthetic  
772 aperture radar imagery - Implications for post-fire tree recruitment. *Remote Sensing of Environment*, 108(1),  
773 42–58. <https://doi.org/10.1016/j.rse.2006.10.020>
- 774 Kettridge, N., Thompson, D. K., & Waddington, J. M. (2012). Impact of wildfire on the thermal behavior of  
775 northern peatlands: Observations and model simulations. *Journal of Geophysical Research: Biogeosciences*,  
776 117(G2), G02014. <https://doi.org/10.1029/2011JG001910>
- 777 Kettridge, N., Lukenbach, M. C., Hokanson, K. J., Hopkinson, C., Devito, K. J., Petrone, R. M., ... Waddington, J.  
778 M. (2017). Low Evapotranspiration Enhances the Resilience of Peatland Carbon Stocks to Fire. *Geophysical*  
779 *Research Letters*, 44(18), 2017GL074186. <https://doi.org/10.1002/2017GL074186>
- 780 Kozeny, J. (1927). Über kapillare leitung der wasser in boden. *Royal Academy of Science, Vienna, Proc. Class I*,  
781 136, 271–306.
- 782 Kurylyk, B. L., Hayashi, M., Quinton, W. L., McKenzie, J. M., & Voss, C. I. (2016). Influence of vertical and lateral  
783 heat transfer on permafrost thaw, peatland landscape transition, and groundwater flow. *Water Resources*  
784 *Research*, 52(2), 1286–1305. <https://doi.org/10.1002/2015WR018057>

- 785 Kurylyk, B. L., & Watanabe, K. (2013). The mathematical representation of freezing and thawing processes in  
786 variably-saturated, non-deformable soils. *Advances in Water Resources*, *60*, 160–177.  
787 <https://doi.org/10.1016/j.advwatres.2013.07.016>
- 788 Lebeau, M., & Konrad, J.-M. (2010). A new capillary and thin film flow model for predicting the hydraulic  
789 conductivity of unsaturated porous media. *Water Resources Research*, *46*(12).  
790 <https://doi.org/10.1029/2010WR009092>
- 791 Liljedahl, A. K., Hinzman, L. D., Kane, D. L., Oechel, W. C., Tweedie, C. E., & Zona, D. (2017). Tundra water  
792 budget and implications of precipitation underestimation. *Water Resources Research*, *53*(8), 6472–6486.  
793 <https://doi.org/10.1002/2016WR020001>
- 794 Lique, C., Holland, M. M., Dibike, Y. B., Lawrence, D. M., & Screen, J. A. (2016). Modeling the Arctic freshwater  
795 system and its integration in the global system: Lessons learned and future challenges. *Journal of Geophysical  
796 Research-Biogeosciences*, *121*(3), 540–566. <https://doi.org/10.1002/2015JG003120>
- 797 Liu, H. P., Randerson, J. T., Lindfors, J., & Chapin, F. S. (2005). Changes in the surface energy budget after fire in  
798 boreal ecosystems of interior Alaska: An annual perspective. *Journal of Geophysical Research-Atmospheres*,  
799 *110*(D13), D13101. <https://doi.org/10.1029/2004JD005158>
- 800 Lukenbach, M. C., Devito, K. J., Kettridge, N., Petrone, R. M., & Waddington, J. M. (2016). Burn severity alters  
801 peatland moss water availability: implications for post-fire recovery. *Ecohydrology*, *9*(2), 341–353.  
802 <https://doi.org/10.1002/eco.1639>
- 803 Mack, M. C., Bret-Harte, M. S., Hollingsworth, T. N., Jandt, R. R., Schuur, E. A. G., Shaver, G. R., & Verbyla, D.  
804 L. (2011). Carbon loss from an unprecedented Arctic tundra wildfire. *Nature*, *475*(7357), 489–492.  
805 <https://doi.org/10.1038/nature10283>
- 806 McClelland, J. W., Holmes, R. M., Peterson, B. J., & Stieglitz, M. (2004). Increasing river discharge in the Eurasian  
807 Arctic: Consideration of dams, permafrost thaw, and fires as potential agents of change. *Journal of Geophysical  
808 Research-Atmospheres*, *109*(D18), D18102. <https://doi.org/10.1029/2004JD004583>
- 809 McKay, M. D., Beckman, R. J., & Conover, W. J. (1979). A Comparison of Three Methods for Selecting Values of  
810 Input Variables in the Analysis of Output from a Computer Code. *Technometrics*, *21*(2), 239–245.  
811 <https://doi.org/10.2307/1268522>
- 812 McKenzie, J. M., Voss, C. I., & Siegel, D. I. (2007). Groundwater flow with energy transport and water–ice phase  
813 change: Numerical simulations, benchmarks, and application to freezing in peat bogs. *Advances in Water  
814 Resources*, *30*(4), 966–983. <https://doi.org/10.1016/j.advwatres.2006.08.008>
- 815 McKenzie, J. M., & Voss, C. I. (2013). Permafrost thaw in a nested groundwater–flow system. *Hydrogeology  
816 Journal*, *21*(1), 299–316. <https://doi.org/10.1007/s10040-012-0942-3>
- 817 Minsley, B. J., Pastick, N. J., Wylie, B. K., Brown, D. R. N., & Kass, M. A. (2016). Evidence for nonuniform  
818 permafrost degradation after fire in boreal landscapes. *Journal of Geophysical Research-Earth Surface*, *121*(2),  
819 320–335. <https://doi.org/10.1002/2015JF003781>
- 820 Mirus, B. B., Ebel, B. A., Mohr, C. H., & Zegre, N. (2017). Disturbance Hydrology: Preparing for an Increasingly  
821 Disturbed Future. *Water Resources Research*, *53*(12), 10007–10016. <https://doi.org/10.1002/2017WR021084>
- 822 Naasz, R., Michel, J.-C., & Charpentier, S. (2005). Measuring Hysteretic Hydraulic Properties of Peat and Pine Bark  
823 using a Transient Method. *Soil Science Society of America Journal*, *69*(1), 13–22.  
824 <https://doi.org/10.2136/sssaj2005.0013>
- 825 Nash, J. E., & Sutcliffe, J. V. (1970). River flow forecasting through conceptual models part I — A discussion of  
826 principles. *Journal of Hydrology*, *10*(3), 282–290. [https://doi.org/10.1016/0022-1694\(70\)90255-6](https://doi.org/10.1016/0022-1694(70)90255-6)
- 827 Nicolosky, D. J., & Romanovsky, V. E. (2018). Modeling long-term permafrost degradation. *Journal of Geophysical  
828 Research: Earth Surface*. <https://doi.org/10.1029/2018JF004655>
- 829 Petrone, K. C., Hinzman, L. D., Shibata, H., Jones, J. B., & Boone, R. D. (2007). The influence of fire and  
830 permafrost on sub-arctic stream chemistry during storms. *Hydrological Processes*, *21*(4), 423–434.  
831 <https://doi.org/10.1002/hyp.6247>
- 832 Quinton, W. L., Hayashi, M., & Carey, S. K. (2008). Peat hydraulic conductivity in cold regions and its relation to  
833 pore size and geometry. *Hydrological Processes*, *22*(15), 2829–2837. <https://doi.org/10.1002/hyp.7027>

- 834 Quinton, W. L., Hayashi, M., & Chasmer, L. E. (2011). Permafrost-thaw-induced land-cover change in the Canadian  
835 subarctic: implications for water resources. *Hydrological Processes*, 25(1), 152–158.  
836 <https://doi.org/10.1002/hyp.7894>
- 837 Quinton, W. L., Gray, D. M., & Marsh, P. (2000). Subsurface drainage from hummock-covered hillslopes in the  
838 Arctic tundra. *Journal of Hydrology*, 237(1), 113–125. [https://doi.org/10.1016/S0022-1694\(00\)00304-8](https://doi.org/10.1016/S0022-1694(00)00304-8)
- 839 R Core Team. (2018). R: A language and environment for statistical computing (Version 3.4.4). Vienna, Austria: R  
840 Foundation for Statistical Computing. Retrieved from <https://www.R-project.org/>
- 841 Rocha, A. V., Shaver, G. R., & Hobbie, J. (2008a). AmeriFlux US-An1 Anaktuvuk River Moderate Burn. Retrieved  
842 February 27, 2017, from <http://dx.doi.org/10.17190/AMF/1246143>
- 843 Rocha, A. V., Shaver, G. R., & Hobbie, J. (2008b). AmeriFlux US-An1 Anaktuvuk River Severe Burn. Retrieved  
844 February 27, 2017, from <http://dx.doi.org/10.17190/AMF/1246142>
- 845 Rocha, A. V., Shaver, G. R., & Hobbie, J. (2008c). AmeriFlux US-An1 Anaktuvuk River Unburned. Retrieved  
846 February 27, 2017, from <http://dx.doi.org/10.17190/AMF/1246144>
- 847 Rocha, A. V., & Shaver, G. R. (2009). Advantages of a two band EVI calculated from solar and photosynthetically  
848 active radiation fluxes. *Agricultural and Forest Meteorology*, 149(9), 1560–1563.  
849 <https://doi.org/10.1016/j.agrformet.2009.03.016>
- 850 Rocha, A. V., & Shaver, G. R. (2011a). Burn severity influences postfire CO<sub>2</sub> exchange in arctic tundra. *Ecological  
851 Applications*, 21(2), 477–489. <https://doi.org/10.1890/10-0255.1>
- 852 Rocha, A. V., & Shaver, G. R. (2011b). Postfire energy exchange in arctic tundra: the importance and climatic  
853 implications of burn severity. *Global Change Biology*, 17(9), 2831–2841. <https://doi.org/10.1111/j.1365-2486.2011.02441.x>
- 854
- 855 Rocha, A. V., & Shaver, G. R. (2015, December 14). Anaktuvuk River fire scar thaw depth measurements during the  
856 2008 to 2014 growing season. Retrieved February 8, 2017, from  
857 <http://dx.doi.org/10.6073/pasta/93121fc86e6fbcf88de4a9350609aed6>
- 858 Romanovsky, V. E., Ping, C.-L., Seybold, C., & Harms, D. (2017). Toolik Soil Climate Station. Retrieved March  
859 27, 2017, from [https://www.nrcs.usda.gov/wps/portal/nrcs/detail/soils/home/?cid=NRCS142P2\\_053712](https://www.nrcs.usda.gov/wps/portal/nrcs/detail/soils/home/?cid=NRCS142P2_053712)
- 860 Schwärzel, K., Šimůnek, J., Stoffregen, H., Wessolek, G., Genuchten, V., & Th, M. (2006). Estimation of the  
861 Unsaturated Hydraulic Conductivity of Peat Soils. *Vadose Zone Journal*, 5(2), 628–640.  
862 <https://doi.org/10.2136/vzj2005.0061>
- 863 Semenova, O., Lebedeva, L., Volkova, N., Korenev, I., Forkel, M., Eberle, J., & Urban, M. (2015). Detecting  
864 immediate wildfire impact on runoff in a poorly-gauged mountainous permafrost basin. *Hydrological Sciences  
865 Journal-Journal Des Sciences Hydrologiques*, 60(7–8), 1225–1241.  
866 <https://doi.org/10.1080/02626667.2014.959960>
- 867 Serbin, S. P., Singh, A., McNeil, B. E., Kingdon, C. C., & Townsend, P. A. (2014). Spectroscopic determination of  
868 leaf morphological and biochemical traits for northern temperate and boreal tree species. *Ecological  
869 Applications*, 24(7), 1651–1669. <https://doi.org/10.1890/13-2110.1>
- 870 Shaver, G. R., & Rocha, A. V. (2015a, December 14). Anaktuvuk River Burn Eddy Flux Measurements, 2008  
871 Moderate Site, North Slope Alaska. Retrieved February 8, 2017, from  
872 <http://dx.doi.org/10.6073/pasta/19e3802d6738c4b30cf09188a2551b10>
- 873 Shaver, G. R., & Rocha, A. V. (2015b, December 14). Anaktuvuk River Burn Eddy Flux Measurements, 2008  
874 Severe Site, North Slope Alaska. Retrieved February 8, 2017, from  
875 <http://dx.doi.org/10.6073/pasta/724bd68e01ee9a59b05cdee5cfa14bbd>
- 876 Shaver, G. R., & Rocha, A. V. (2015c, December 14). Anaktuvuk River Burn Eddy Flux Measurements, 2008  
877 Unburned Site, North Slope Alaska. Retrieved February 8, 2017, from  
878 <http://dx.doi.org/10.6073/pasta/48f728d2fe75541c8f4f6827ce8dc039>
- 879 Shaver, G. R., & Rocha, A. V. (2015d, December 14). Anaktuvuk River Burn Eddy Flux Measurements, 2009  
880 Moderate Site, North Slope Alaska. Retrieved February 8, 2017, from  
881 <http://dx.doi.org/10.6073/pasta/3d912564439309bdf17bc75866179312>

- 882 Shaver, G. R., & Rocha, A. V. (2015e, December 14). Anaktuvuk River Burn Eddy Flux Measurements, 2009  
 883 Severe Site, North Slope Alaska. Retrieved February 8, 2017, from  
 884 <http://dx.doi.org/10.6073/pasta/5554a6eda8082f933709e547811b85dc>
- 885 Shaver, G. R., & Rocha, A. V. (2015f, December 14). Anaktuvuk River Burn Eddy Flux Measurements, 2009  
 886 Unburned Site, North Slope Alaska. Retrieved February 8, 2017, from  
 887 <http://dx.doi.org/10.6073/pasta/aeb3845bf779ca10f13930e1d6c90105>
- 888 Shaver, G. R., & Rocha, A. V. (2015g, December 14). Anaktuvuk River Burn Eddy Flux Measurements, 2010  
 889 Moderate Site, North Slope Alaska. Retrieved February 8, 2017, from  
 890 <http://dx.doi.org/10.6073/pasta/abee3157f007a794edb3414e1280d71b>
- 891 Shaver, G. R., & Rocha, A. V. (2015h, December 14). Anaktuvuk River Burn Eddy Flux Measurements, 2010  
 892 Severe Site, North Slope Alaska. Retrieved February 8, 2017, from  
 893 <http://dx.doi.org/10.6073/pasta/2330a47db633130f0972bc134e714066>
- 894 Shaver, G. R., & Rocha, A. V. (2015i, December 14). Anaktuvuk River Burn Eddy Flux Measurements, 2010  
 895 Unburned Site, North Slope Alaska. Retrieved February 8, 2017, from  
 896 <http://dx.doi.org/10.6073/pasta/ff790bd426b262aa7d818ad7f0b2d2a4>
- 897 Shaver, G. R., & Rocha, A. V. (2015j, December 14). Anaktuvuk River Burn Eddy Flux Measurements, 2011  
 898 Moderate Site, North Slope Alaska. Retrieved February 8, 2017, from  
 899 <http://dx.doi.org/10.6073/pasta/f7e7d023fbac22d83ad0c2e4ce191650>
- 900 Shaver, G. R., & Rocha, A. V. (2015k, December 14). Anaktuvuk River Burn Eddy Flux Measurements, 2011  
 901 Severe Site, North Slope Alaska. Retrieved February 8, 2017, from  
 902 <http://dx.doi.org/10.6073/pasta/d384b812a12e5cfa7fdbb4032cf1abb2>
- 903 Shaver, G. R., & Rocha, A. V. (2015l, December 14). Anaktuvuk River Burn Eddy Flux Measurements, 2011  
 904 Unburned Site, North Slope Alaska. Retrieved February 8, 2017, from  
 905 <http://dx.doi.org/10.6073/pasta/913d3843eb71f27bac3f9c97df61573e>
- 906 Shaver, G. R., & Rocha, A. V. (2015m, December 14). Anaktuvuk River Burn Eddy Flux Measurements, 2012  
 907 Moderate Site, North Slope Alaska. Retrieved February 8, 2017, from  
 908 <http://dx.doi.org/10.6073/pasta/b5c015dbf57ba3b3ec3ee1d95a663fc5>
- 909 Shaver, G. R., & Rocha, A. V. (2015n, December 14). Anaktuvuk River Burn Eddy Flux Measurements, 2012  
 910 Severe Site, North Slope Alaska. Retrieved February 8, 2017, from  
 911 <http://dx.doi.org/10.6073/pasta/ed412a2a1940af95ab4611212200a5c5>
- 912 Shaver, G. R., & Rocha, A. V. (2015o, December 14). Anaktuvuk River Burn Eddy Flux Measurements, 2012  
 913 Unburned Site, North Slope Alaska. Retrieved February 8, 2017, from  
 914 <http://dx.doi.org/10.6073/pasta/67188afe29827f8b3c0277753b2a956a>
- 915 Sherwood, J. H., Kettridge, N., Thompson, D. K., Morris, P. J., Silins, U., & Waddington, J. M. (2013). Effect of  
 916 drainage and wildfire on peat hydrophysical properties. *Hydrological Processes*, 27(13), 1866–1874.  
 917 <https://doi.org/10.1002/hyp.9820>
- 918 da Silva, F. F., Wallach, R., & Chen, Y. (1993). Hydraulic properties of sphagnum peat moss and tuff (scoria) and  
 919 their potential effects on water availability. *Plant and Soil*, 154(1), 119–126.  
 920 <https://doi.org/10.1007/BF00011080>
- 921 Smith, S. L., Riseborough, D. W., & Bonnaventure, P. P. (2015). Eighteen Year Record of Forest Fire Effects on  
 922 Ground Thermal Regimes and Permafrost in the Central Mackenzie Valley, NWT, Canada. *Permafrost and*  
 923 *Periglacial Processes*, 26(4), 289–303. <https://doi.org/10.1002/ppp.1849>
- 924 The Inkscape Team. (2015). Inkscape (Version 0.91). Retrieved from <https://inkscape.org/en/>
- 925 Thompson, D. K., & Waddington, J. M. (2013). Peat properties and water retention in boreal forested peatlands  
 926 subject to wildfire. *Water Resources Research*, 49(6), 3651–3658. <https://doi.org/10.1002/wrcr.20278>
- 927 Thompson, D. K., Benscoter, B. W., & Waddington, J. M. (2014). Water balance of a burned and unburned forested  
 928 boreal peatland. *Hydrological Processes*, 28(24), 5954–5964. <https://doi.org/10.1002/hyp.10074>
- 929 Treat, C. C., Wissler, D., Marchenko, S., & Froelking, S. (2013). Modelling the effects of climate change and  
 930 disturbance on permafrost stability in northern organic soils. *Mires and Peat*, 12, 2.

- 931 Van Genuchten, M. T. (1980). A closed-form equation for predicting the hydraulic conductivity of unsaturated soils.  
932 *Soil Science Society of America Journal*, 44(5), 892.  
933 <https://doi.org/10.2136/sssaj1980.03615995004400050002x>
- 934 Voss, C. I. (2011a). Editor's message: Groundwater modeling fantasies —part 1, adrift in the details. *Hydrogeology*  
935 *Journal*, 19(7), 1281–1284. <https://doi.org/10.1007/s10040-011-0789-z>
- 936 Voss, C. I. (2011b). Editor's message: Groundwater modeling fantasies—part 2, down to earth. *Hydrogeology*  
937 *Journal*, 19(8), 1455–1458. <https://doi.org/10.1007/s10040-011-0790-6>
- 938 Voss, C. I., & Provost, A. M. (2010). *SUTRA: A Model for Saturated-Unsaturated Variable-Density Ground-Water*  
939 *Flow with Solute or Energy Transport* (No. Water Resources Investigations Report 02-4231). Reston VA: U.S.  
940 Geological Survey.
- 941 Walter, M. T., Brooks, E. S., McCool, D. K., King, L. G., Molnau, M., & Boll, J. (2005). Process-based snowmelt  
942 modeling: does it require more input data than temperature-index modeling? *Journal of Hydrology*, 300(1), 65–  
943 75. <https://doi.org/10.1016/j.jhydrol.2004.05.002>
- 944 Walvoord, M. A., & Kurylyk, B. L. (2016). Hydrologic Impacts of Thawing Permafrost-A Review. *Vadose Zone*  
945 *Journal*, 15(6). <https://doi.org/10.2136/vzj2016.01.0010>
- 946 Walvoord, M. A., Voss, C. I., & Wellman, T. P. (2012). Influence of permafrost distribution on groundwater flow in  
947 the context of climate-driven permafrost thaw: Example from Yukon Flats Basin, Alaska, United States. *Water*  
948 *Resources Research*, 48(7), W07524. <https://doi.org/10.1029/2011WR011595>
- 949 Watanabe, K., & Flury, M. (2008). Capillary bundle model of hydraulic conductivity for frozen soil. *Water*  
950 *Resources Research*, 44(12). <https://doi.org/10.1029/2008WR007012>
- 951 Wellman, T. P., Voss, C. I., & Walvoord, M. A. (2013). Impacts of climate, lake size, and supra- and sub-permafrost  
952 groundwater flow on lake-talik evolution, Yukon Flats, Alaska (USA). *Hydrogeology Journal*, 21(1), 281–298.  
953 <https://doi.org/10.1007/s10040-012-0941-4>
- 954 Wickham, H. (2009). *ggplot2: Elegant Graphics for Data Analysis*. Springer-Verlag New York. Retrieved from  
955 <http://ggplot2.org>
- 956 Wood, S. N. (2003). Thin-plate regression splines. *Journal of the Royal Statistical Society (B)*, 65(1), 95–114.
- 957 Wood, S. N. (2011). Fast stable restricted maximum likelihood and marginal likelihood estimation of  
958 semiparametric generalized linear models. *Journal of the Royal Statistical Society (B)*, 73(1), 3–36.
- 959 Wood, S. N. (2017). *Generalized Additive Models: An Introduction with R (2nd edition)*. Chapman and Hall/CRC.
- 960 Wrona, F. J., Johansson, M., Culp, J. M., Jenkins, A., Mård, J., Myers-Smith, I. H., ... Wookey, P. A. (2016).  
961 Transitions in Arctic ecosystems: Ecological implications of a changing hydrological regime. *Journal of*  
962 *Geophysical Research: Biogeosciences*, 121(3), 2015JG003133. <https://doi.org/10.1002/2015JG003133>
- 963 Yi, S., McGuire, A. D., Harden, J., Kasischke, E. S., Manies, K., Hinzman, L., ... Kim, Y. (2009). Interactions  
964 between soil thermal and hydrological dynamics in the response of Alaska ecosystems to fire disturbance.  
965 *Journal of Geophysical Research-Biogeosciences*, 114, G02015. <https://doi.org/10.1029/2008JG000841>
- 966 Zambrano-Bigiarini, M. (2014). hydroGOF: Goodness-of-fit functions for comparison of simulated and observed  
967 hydrological time series (Version 0.3-8). Retrieved from <https://CRAN.R-project.org/package=hydroGOF>
- 968 Zhang, Y., Chen, W., & Cihlar, J. (2003). A process-based model for quantifying the impact of climate change on  
969 permafrost thermal regimes. *Journal of Geophysical Research: Atmospheres*, 108(D22), 4695.  
970 <https://doi.org/10.1029/2002JD003354>
- 971 Zhang, Y., Carey, S. K., Quinton, W. L., Janowicz, J. R., Pomeroy, J. W., & Flerchinger, G. N. (2010). Comparison  
972 of algorithms and parameterisations for infiltration into organic-covered permafrost soils. *Hydrology and Earth*  
973 *System Sciences*, 14(5), 729–750. <https://doi.org/10.5194/hess-14-729-2010>
- 974 Zhang, Y., Wolfe, S. A., Morse, P. D., Olthof, I., & Fraser, R. H. (2015). Spatiotemporal impacts of wildfire and  
975 climate warming on permafrost across a subarctic region, Canada. *Journal of Geophysical Research-Earth*  
976 *Surface*, 120(11), 2338–2356. <https://doi.org/10.1002/2015JF003679>
- 977 Zhuang, Q., McGuire, A. D., O'Neill, K. P., Harden, J. W., Romanovsky, V. E., & Yarie, J. (2002). Modeling soil  
978 thermal and carbon dynamics of a fire chronosequence in interior Alaska. *Journal of Geophysical Research-*  
979 *Atmospheres*, 108(D1), 8147. <https://doi.org/10.1029/2001JD001244>

- 980 Zipper, S. C., Dallemagne, T., Gleeson, T., Boerman, T. C., & Hartmann, A. (2018). Groundwater Pumping Impacts  
981 on Real Stream Networks: Testing the Performance of Simple Management Tools. *Water Resources Research*.  
982 <https://doi.org/10.1029/2018WR022707>
- 983 Zipper, S. C., & Loheide, S. P. (2014). Using evapotranspiration to assess drought sensitivity on a subfield scale  
984 with HRMET, a high resolution surface energy balance model. *Agricultural and Forest Meteorology*, *197*, 91–  
985 102. <https://doi.org/10.1016/j.agrformet.2014.06.009>
- 986 Zipper, S. C., Schatz, J., Singh, A., Kucharik, C. J., Townsend, P. A., & Loheide, S. P. (2016). Urban heat island  
987 impacts on plant phenology: intra-urban variability and response to land cover. *Environmental Research*  
988 *Letters*, *11*(5), 054023. <https://doi.org/10.1088/1748-9326/11/5/054023>
- 989 Zipper, S. C., Schatz, J., Kucharik, C. J., & Loheide, S. P. (2017). Urban heat island-induced increases in  
990 evapotranspirative demand. *Geophysical Research Letters*, *44*(2), 2016GL072190.  
991 <https://doi.org/10.1002/2016GL072190>

992